Advanced Automotive Radar Front-end

Based on Gapwaveguide Technology

QIANNAN REN

Advanced Automotive Radar Front-end

Based on Gapwaveguide Technology

Department of Electrical Engineering
Chalmers University of Technology
SE-412 96 Gothenburg, Sweden
Phone: +46 (0)31 772 1000

To my family.

Advanced Automotive Radar Front-end
Based on Gapwaveguide Technology
Qiannan Ren
Department of Electrical Engineering
Chalmers University of Technology

Abstract

The pursuit of higher levels of autonomous driving necessitates the utilization of advanced radar sensors that possess improved environmental perception capabilities. Consequently, next-generation automotive radars require sophisticated antenna systems with high efficiency, thereby making waveguide antennas a more viable choice. In this context, it has been observed that gapwaveguides exhibit superior performance in comparison to traditional waveguides, particularly in terms of assembly reliability, when employed in the development of multi-layer waveguide antennas. Within the scope of this thesis, the primary objective is to comprehensively explore the design of front-ends for cutting-edge automotive radar sensors by leveraging the potential of gapwaveguide technology.

The initial aspect of this thesis involves an exploration of integration techniques capable of achieving high performance in waveguide-based RF front-ends. In particular, the thesis introduces novel vertical gapwaveguide-to-microstrip transitions that facilitate the integration of RF front-ends featuring multi-layer configurations. Furthermore, this thesis introduces radar transceivers equipped with built-in waveguide-to-microstrip transitions, known as launcher-in-package, along with an imaging radar antenna featuring customized interconnections explicitly designed utilizing gapwaveguide technology to interface with the transceivers.

Secondly, in light of the utilization of radar sensors incorporating orthogonal dual polarizations on the transmitting and/or receiving ends, an opportunity arises to acquire polarimetric information from the surrounding environment, thereby representing a promising advancement in the realm of autonomous driving. This thesis presents novel antenna designs based on gapwaveguide technology for polarimetric radar sensors. An 8×8 planar array utilizing double grooved circular waveguide polarizers is introduced, specifically designed for fixed beam, high gain polarimetric sensing applications. In addition, this

thesis presents a polarimetric radar sensor that utilizes a MIMO configuration featuring single-CP transmitting antennas and dual-CP receiving antennas. The antenna design incorporates series-fed septum polarizers, which offer low-profile characteristics.

In summary, this thesis undertakes a comprehensive investigation into the designs of advanced automotive radar front-ends utilizing gapwaveguide technology. The study explores the advancements in terms of integration techniques and polarimetric capability, demonstrating the potential of gapwaveguide technology for the practical implementation of waveguide-based RF front-ends. The utilization of such front-ends can significantly enhance the capabilities of autonomous driving systems.

List of Publications

This thesis is based on the following publications:

[A] **Qiannan Ren**, Ashraf Uz Zaman, Jian Yang, Vessen Vassilev, Carlo Bencivenni, "Novel Integration Techniques for Gap Waveguides and MMICs Suitable for Multilayer Waveguide Applications". *IEEE Transactions on Microwave Theory and Techniques*, vol. 70, no. 9, pp. 4120-4128, Sept. 2022. 0018-9480 © 2022 IEEE DOI: 10.1109/TMTT.2022.3194204.

[B] **Qiannan Ren**, Ashraf Uz Zaman, Jian Yang, "Dual-Circularly Polarized Array Antenna Based on Gap Waveguide Utilizing Double-grooved Circular Waveguide Polarizer". *IEEE Transactions on Antennas and Propagation*, vol. 70, no. 11, pp. 10436-10444, Nov. 2022. 0018-926X © 2022 IEEE DOI: 10.1109/TAP.2022.3195458.

[C] **Qiannan Ren**, Carlo Bencivenni, Giorgio Carluccio, Harshitha Thippur Shivamurthy, Anton de Graauw, Feike Jansen, Jian Yang, Ashraf Uz Zaman, "Gapwaveguide Automotive Imaging Radar Antenna With Launcher in Package Technology". *IEEE Access*, vol. 11, pp. 37483-37493, 2023. © CCBY-NC-ND DOI: 10.1109/ACCESS.2023.3266958.

[D] **Qiannan Ren**, Olof Eriksson, Carina Marcus, Prateek Thalya, Rustem Elezovic, Carlo Bencivenni, Marcus Hasselblad, Jian Yang, Zhaorui Zang, Ashraf Uz Zaman, "An Automotive Polarimetric Radar Sensor with Circular Polarization Based on Gapwaveguide Technology". *Submitted to IEEE Transactions on Microwave Theory and Techniques*.

Other publications by the author, not included in this thesis, are:

[E] **Q. Ren**, A. U. Zaman, J. Yang, V. Vassilev and C. Bencivenni, "Millimeter-Wave Vertical Transitions Between Ridge Gap Waveguides and Microstrip Lines for Integration of MMIC with Slot Array". *2021 15th European Conference on Antennas and Propagation (EuCAP)*, Dusseldorf, Germany, 2021, pp. 1-4, doi: 10.23919/EuCAP51087.2021.9411273.

[F] **Q. Ren**, A. U. Zaman and J. Yang, "A Dual Circularly Polarized Array Antenna for Ka-Band Satellite Communications". *2021 International Sympo-*

sium on Antennas and Propagation (ISAP), Taipei, Taiwan, 2021, pp. 1-2, doi: 10.23919/ISAP47258.2021.9614491.

Acknowledgments

I would like to express my deepest gratitude to my supervisor, Associate Prof. Ashraf Uz Zaman, for his support and guidance throughout my research journey. His creative ideas and constructive feedback have been invaluable in resolving challenges and clarifying my research direction. I am also grateful to my examiner, Prof. Jian Yang, for his encouragement and patience during the project.

I extend my sincere thanks to my manager, Prof. Marianna Ivashina, for her considerate guidance during my Ph.D. studies. I am also grateful to Prof. Rob Maaskant for generously sharing his valuable teaching experience with me. I would also like to express my sincere thanks to Dr. Oleg Iupikov, Dr. Pavlo Krasov, and Dr. Artem Vilenskiy for their generous support throughout the years.

I am grateful to the members of the Antenna Systems Group for creating a productive and collaborative working environment. I would like to thank Dr. Jinlin Liu, Dr. Madeleine Kildal, Dr. Sadegh Mansouri Moghaddam, Dr. Artem Roev, Dr. Wan-chun Liao, Dr. Navid Amani, and Dr. Jonas Flygare for sharing their valuable experience and insights during my early Ph.D. stages. I am also thankful to Zhaorui, Yingqi, Usman, Mustafa, Viktor, Dmitrii, Prabhat, Mu, Raha, Yuqing, Enlin, and Jin for their assistance in my research.

I would like to extend special thanks to my co-supervisor, Dr. Carlo Bencivenni from Gapwaves AB, for his patient supervision. I am also grateful to Associate Prof. Vessen Vassilev from the Department of Microtechnology and Nanoscience for his caring support.

I would like to acknowledge the contributions of everyone involved in the FORWARD project, including Marcus Hasselblad from Gapwaves, Robert Moestam from CEVT, and Olof Eriksson, Prateek Thaly, Rustem Elezovic, Carina Marcus from Veoneer.

Lastly, I would like to express my deepest appreciation to my family for their selfless support and boundless love throughout this journey. Their encouragement has been my pillar of strength.

Acronyms

ADAS:	Advanced driver assistance systems
V2X:	Vehicle to everything
LiDAR:	Light detection and ranging
FoV:	Field of view
ACC:	Adaptive cruise control
LRR:	Long-range radar
MRR:	Medium-range radar
SRR:	Short-range radar
SiP:	System in package
TX:	Transmitters
RX:	Receivers
LiP:	Launcher in package
eWLB:	Embedded wafer level ball grid array
PCB:	Print circuit board
LP:	Linear polarization
CP:	Circular polarization
MIMO:	Multi input Multi output
SAR:	synthetic aperture radar
PEC:	Perfect electric conductor
PMC:	Perfect magnetic conductor
CNC:	Computer numerical control

EDM:	Electric discharge machining
RF:	Radio frequency
IF:	Intermediate frequency
LO:	Local oscillator
PLL:	Phase-locked loop
ADC:	Analog-to-digital converter
MCU:	Micro-controller unit
DSP:	Digital signal processor
AoP:	Antenna on package
BGA:	Ball grid array
GCPW:	Grounded coplanar waveguide
GGW:	Groove gap waveguide
HPGGW:	Horizontally polarized gap waveguide
RGW:	Ridge gap waveguide
IMGW:	Inverted microstrip gap waveguide
MMIC:	Monolithic microwave integrated circuit
RHCP:	Right hand circular polarization
LHCP:	Left hand circular polarization
AR:	Axial ratio
HPBW:	Half power beam width
DoA:	Direction of arrival
VA:	Virtual array
RCS:	Radar cross section
TDM:	Time division multiplexing

Contents

Part I

Overview

Introduction

This chapter provides an overview of the research background related to advanced automotive radar front-ends. It begins by providing an introduction to autonomous driving, outlining the levels of automation. The concept of polarimetric sensing is also introduced, highlighting its relevance to automotive radar systems. Additionally, the fundamentals of gap waveguide technology are elaborated, emphasizing its significance in addressing challenges encountered in high-frequency applications. Lastly, an outline of the thesis is presented, giving a glimpse into the content of the research.

1.1 Overview of Autonomous Driving

The Society of Automotive Engineers (SAE) has formulated a comprehensive framework outlining six distinct levels of autonomous driving, spanning from Level 0 (complete reliance on human operation) to Level 5 (complete automation without human intervention). This framework is presently employed on a global scale by regulators and manufacturers as a standardized mechanism for evaluating and classifying autonomous driving vehicles, as listed in Table. 1.1 [1].

Table 1.1: Automation Levels [1]

Level	Name	Narrative definition	Execution of steering and acceleration/ deceleration	Monitoring of driving environment	Fallback performance of dynamic driving task	System capability (driving modes)
Human driver monitors the driving environment						
0	No automation	The full-time performance by the human driver of all aspects of the dynamic driving task, even when "enhanced by warning or intervention systems"	Human driver	Human driver	Human driver	N/a
1	Driver assistance	The driving mode-specific execution by a driver assistance system of either steering or acceleration /deceleration	Human driver and system			Some driving modes
2	Partial automation	The driving mode-specific execution by one or more driver assistance systems of both steering and acceleration/deceleration	System			
Automated driving system monitors the driving environment						
3	Conditional automation	With the expectation that the human driver will respond appropriately to a request to intervene	System	System	Human driver	Some driving modes
4	High automation	Even if a human driver does not respond appropriately to a request to intervene the car can pull over safely by guiding system	System		System	Many driving modes
5	Full automation	Under all roadway and environmental conditions that can be managed by a human driver	System			All driving modes

Table 1.2: A comparison of the commonly employed sensors in self-driving cars: cameras, LiDAR, and radar, based on technical characteristics and other external factors. The "✓" symbol indicates that the sensor operates competently under the specific factor. The "∼" symbol indicates that the sensor performs reasonably well under the specific factor. The "✗" symbol indicates that the sensor does not operate well under the specific factor relative to other sensors [2].

Factors	Camera	LiDAR	Radar	Fusion
Range	∼	∼	✓	✓
Resolution	✓	∼	✗	✓
Distance Accuracy	∼	✓	✓	✓
Velocity	∼	✗	✓	✓
Color Perception, e.g. traffic lights	✓	✗	✗	✓
Object Detection	∼	✓	✓	✓
Object Classification	✓	∼	✗	✓
Lane Detection	✓	✗	✗	✓
Obstacle Edge Detection	✓	✓	✗	✓
Illumination Conditions	✗	✓	✓	✓
Weather Conditions	✗	∼	✓	✓

Adaptive Cruise Control (ACC), an advanced functionality capable of autonomously modifying vehicle speed to ensure a safe following distance from preceding vehicles, is classified as the least complex level of automation (Level 1). A significant portion of the currently available vehicles featuring Advanced Driver Assistance Systems (ADAS) are positioned within the Level 2 category of autonomous driving, such as Tesla's Enhanced Autopilot, Volvo's Pilot Assist, etc. Level 3 represents a remarkable advancement in the realm of autonomous driving, wherein the system assumes the primary driving role while human drivers are expected to intervene only when assistance is specifically requested. However, the realization of Level 3 autonomous driving is still impeded by a variety of regulatory challenges, indicating that a considerable amount of time may elapse before it can be widely adopted. The advent of Level 4 autonomous driving poses significant challenges to legislation and infrastructures, primarily due to the extensive involvement of Vehicle-to-

Everything (V2X) communication. Level 5 autonomous vehicles are characterized by their complete automation, making them particularly attractive for implementation in the domain of public transportation.

The implementation of autonomous driving vehicles requires the integration of numerous sensors to enable the vehicle to perceive its surroundings effectively. These sensors involve a range of technologies, including video cameras, radars, light detection and ranging (LiDAR) sensors, as well as ultrasonic sensors [3], [4]. The sensory data acquired from the aforementioned sensors is processed by the autonomous system to identify key elements in the environment, such as navigation paths, traffic signs, and obstacles. Table 1.2 presents a comparison of various sensors, highlighting their strengths and weaknesses under different scenarios [2]. Sensor fusion techniques are widely regarded as the most reliable solutions for autonomous driving, as they combine the data outputs of multiple sensors in a complementary manner. Sensor fusion systems are able to benefit from the strengths of various sensors, meanwhile reduce detection uncertainties. For example, the fusion of cameras and radar sensors allows for the generation of high-resolution images while also providing valuable information about the relative range and velocities of detected obstacles.

Radar sensors emit electromagnetic waves within their designated field of view (FoV), which subsequently interact with objects in the vicinity. The sensors then receive the scattered waves reflected by these targets and employ signal processing techniques to extract valuable information. Radar sensors have an advantage over light detection-based sensors when it comes to adverse weather conditions such as fog, dust, snow, or poor lighting. This is because electromagnetic waves, which are used by radar sensors, are less susceptible to interference and degradation caused by these environmental factors. Moreover, the cost of radar sensors is experiencing a decline as a result of mass production, making them increasingly appealing for various industrial applications. A significant number of autonomous vehicles available in the market are equipped with multiple radar sensors strategically positioned at various locations on the vehicle. These locations commonly include front bumpers, rear bumpers, side mirrors, front grilles, etc. Aforementioned qualities of the radar sensors make them indispensable in sensor fusion systems [5], [6].

The 77 GHz band is widely used for automotive radar sensor design due to several key reasons. Firstly, the high frequency of 77 GHz allows for precise

and accurate detection and localization of objects, making it ideal for applications such as collision avoidance and adaptive cruise control. The short wavelength associated with this frequency enables high-resolution imaging, which enhances the radar sensor's ability to distinguish between closely spaced objects. Additionally, the 77 GHz band offers a large available bandwidth, allowing for improved radar performance. Moreover, this frequency band is allocated exclusively for automotive radar systems, reducing the potential for interference from other sources. Overall, the utilization of the 77 GHz band in automotive radar sensor design provides enhanced safety and efficiency, making it a popular choice in the industry [7]–[9]. The primary focus of this thesis is centered around the 77 GHz frequency band.

1.2 Basics of Polarimetric Sensing

Higher levels of vehicle automation demand radar sensors with enhanced perception of the environment [10]. As a result, there has been recent investigations into the use of radar sensors that employ orthogonal dual polarizations on transmitting and/or receiving ends [11]–[13]. This technology allows for the acquisition of polarimetric information from the surrounding environment, resulting in improved target detect-ability and enabling the assessment of road surface conditions. Consequently, the use of polarimetric radar sensors represents a promising advancement in the field of autonomous driving.

Scattering matrix, commonly referred to as S-matrix, is a mathematical representation of how an electromagnetic wave interacts with a target [14]. Elements of the S-matrix are complex numbers that represent amplitude and phase of the electric field components of the scattered wave relative to the incident wave, as indicated in Eqn. 1.1 where $\mathbf{r}$ is the distance vector between the radar sensor and target, $\mathbf{k}$ is the electromagnetic wave number, $\mathbf{E_i}$ and $\mathbf{E_s}$ are the incident and scattered waves respectively. Diagonal elements of the matrix represent amplitudes of the co-polarized components of the scattered wave, while off-diagonal elements represent amplitudes of the cross-polarized components.

$$\mathbf{E_s} = \frac{e^{-j\mathbf{k}\mathbf{r}}}{\sqrt{4\pi}|\mathbf{r}|} \begin{pmatrix} S_{11} & S_{12} \\ S_{21} & S_{22} \end{pmatrix} \mathbf{E_i} \tag{1.1}$$

In the case of a system utilizing a linear polarization (LP) basis, the scattering

matrix entries can be expressed as follows:

$$\begin{pmatrix} \mathbf{E_{s,H}} \\ \mathbf{E_{s,V}} \end{pmatrix} = \frac{e^{-j\mathbf{kr}}}{\sqrt{4\pi}|\mathbf{r}|} \begin{pmatrix} S_{HH} & S_{HV} \\ S_{VH} & S_{VV} \end{pmatrix} \begin{pmatrix} \mathbf{E_{i,H}} \\ \mathbf{E_{i,V}} \end{pmatrix} \tag{1.2}$$

Subscript letters H and V represent horizontal and vertical polarization respectively. Similarly, for a system employing a circular polarization (CP) basis, the scattering matrix entries can be expressed as:

$$\begin{pmatrix} \mathbf{E_{s,L}} \\ \mathbf{E_{s,R}} \end{pmatrix} = \frac{e^{-j\mathbf{kr}}}{\sqrt{4\pi}|\mathbf{r}|} \begin{pmatrix} S_{LL} & S_{LR} \\ S_{RL} & S_{RR} \end{pmatrix} \begin{pmatrix} \mathbf{E_{i,L}} \\ \mathbf{E_{i,R}} \end{pmatrix} \tag{1.3}$$

Subscript letters L and R represent left hand and right hand circular polarization respectively. In [15], three fundamental symmetric scattering objects are proposed, namely the plate, dihedral, and dipole. Scattering matrices for the three basic objects are as follows:

$$S_{\text{plate},LP} = \begin{pmatrix} 1 & 0 \\ 0 & 1 \end{pmatrix} \tag{1.4}$$

$$S_{\text{plate},CP} = \begin{pmatrix} 0 & 1 \\ 1 & 0 \end{pmatrix} \tag{1.5}$$

$$S_{\text{dihedral},LP} = \begin{pmatrix} cos(2\Psi) & sin(2\Psi) \\ sin(2\Psi) & -cos(2\Psi) \end{pmatrix} \tag{1.6}$$

$$S_{\text{dihedral},CP} = \begin{pmatrix} e^{j2\Psi} & 0 \\ 0 & e^{-j2\Psi} \end{pmatrix} \tag{1.7}$$

$$S_{\text{dipole},LP} = \begin{pmatrix} cos^2(\Psi) & cos(\Psi)\,sin(\Psi) \\ cos(\Psi)\,sin(\Psi) & sin^2(\Psi) \end{pmatrix} \tag{1.8}$$

$$S_{\text{dipole},CP} = \frac{1}{2} \begin{pmatrix} e^{j2\Psi} & 1 \\ 1 & e^{-j2\Psi} \end{pmatrix} \tag{1.9}$$

where Ψ represents the inclination angle of the dihedral or dipole.

Existing systems that utilize a single linear polarization (LP) without polarimetric capabilities are limited in their ability to measure the complete scattering matrix. Consequently, these systems fail to capture comprehensive information about the surrounding scenery [16]. As an example, radar systems employing vertical polarization for both transmitting and receiving are unable to detect a dihedral object with an inclination angle of 45°. Additionally, in order to mitigate the risk of encountering blind spots, polarimetric radar systems based on linear polarizations necessitate the implementation

of both horizontal and vertical polarizations at both the transmitter (TX) and receiver (RX) sides. In contrast, according to studies on S-matrix in CP basis, deploying a single CP in the TX end, along with dual CP in the RX end, is a viable strategy for achieving reliable detection, despite being incapable of measuring the full S-matrix [11]. This configuration allows for the acquisition of sufficient polarimetric data while reducing the number of transmitters by half when compared to a fully polarimetric radar system. The redundant transmitters are employed to enlarge the virtual array aperture size with appropriate typologies, which is particularly cost-effective for enhancing the angular resolution.

Polarimetric sensing plays a vital role in various applications such as synthetic aperture radar (SAR) imaging, Doppler weather radar, and road surface monitoring. In autonomous driving applications, the perception of road surface conditions holds significant importance. Recent investigations have explored the use of passive radiometers with polarimetric capabilities to identify road conditions, including dry surfaces, liquid water, and ice on asphalt [17]. Additionally, polarimetric radars have been employed for road recognition purposes [18]–[20]. Recent research has also focused on investigating polarimetric multiple-input multiple-output (MIMO) systems for automotive applications [21], [22]. MIMO systems provide a cost-effective approach to enhance the angular resolution of radar systems by leveraging transmission multiplexing across multiple antennas [23].

1.3 Overview of Gap Waveguide Technologies

The development of waveguide transmission lines stands as a significant milestone in the field of microwave engineering. Initially, it was widely accepted that two conductors were indispensable for the propagation of waves [24]. However, it was not until 1897 that mathematical verification of wave propagation in waveguides with circular and rectangular cross-sections was presented [25]. Subsequently, experimental confirmation of waveguide propagation was provided in 1936, leading to an increased interest and attention towards waveguide technology [26].

Waveguides offer significant advantages such as high power-handling capability and low-loss properties, making them a popular choice in the design of large gain/high efficiency array antennas. However, as the operating frequency

increases and the wavelength shrinks, the fabrication of waveguides becomes more challenging. Traditionally, waveguide modules are manufactured using split-blocks, which are then connected through methods such as screwing. At even higher frequencies, techniques like diffusion bonding and vacuum brazing are employed. However, as the frequency rises, the assembly process becomes critical due to the difficulty of achieving reliable electrical contacts between the split blocks. This necessitates the development of new waveguide technologies that are not only cost-effective but also capable of providing reliable assembly in the millimeter-wave frequency band, surpassing the limitations of common hollow waveguides.

In recent years, gap waveguide technologies have emerged as a promising solution to overcome the challenges mentioned earlier [27]. These technologies have gained significant interest from both industrial and academic communities. To explain the operational principles of a gap waveguide, let's consider a parallel plate structure comprising an upper perfect electric conductor (PEC) plate and a lower perfect magnetic conductor (PMC) plate. As depicted in Fig. 1.1a, no wave propagation occurs between the plates when the separation of the air gap is smaller than a quarter wavelength. However, this limitation can be overcome by incorporating guiding structures on the PMC surface, as illustrated in Fig. 1.1b.
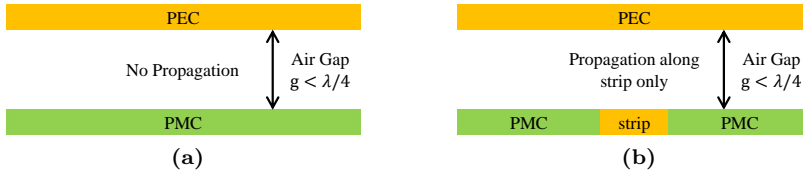
Figure 1.1: Cross section of ideal gap waveguide.

In practical applications, the PMC condition is emulated by incorporating periodic textured structures, such as metal pins or mushroom structures [28], [29]. These structures are responsible for providing the necessary guidance for wave propagation in the gap waveguide. Depending on the specific configuration of the guiding structures, different types of gap waveguide transmission lines can be realized. Fig. 1.2 illustrates some of the commonly used configurations of gap waveguide transmission lines.

The application of gap waveguide technology has led to the development of

various multi-layer waveguide components, including slot arrays, filters, and diplexers, as discussed in multiple studies [30]–[36]. These studies have demonstrated that components based on gap waveguide technology exhibit competitive performance when compared to their conventional waveguide counterparts. Additionally, the utilization of gap waveguide technology enables greater flexibility in designing interconnections between the layers, allowing for improved integration. The integration of mmWave front-ends has also been explored using gap waveguide technology [37]. Gap waveguide integration is a multi-layer integration technique that offers advantages such as non-galvanic contact between the layers, resulting in increased assembly reliability and system robustness [38].

(a)

(b)

(c)

(d)
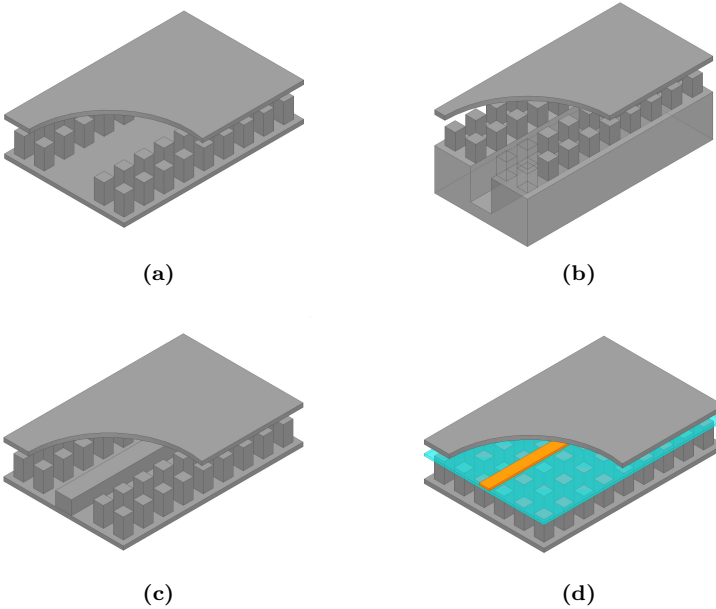
Figure 1.2: Gap waveguide configurations: (a) groove gap waveguide (GGW), (b) horizontally polarized gap waveguide (HPGGW), (c) ridge gap waveguide (RGW), (d) inverted microstrip gap waveguide (IMGW).

Traditionally, computer numerical control (CNC) milling has been commonly employed for fabricating gap waveguide components. However, the

11

increasing cost and time-consuming nature of CNC milling, particularly for producing small features, have posed challenges. To address these issues, alternative low-cost manufacturing techniques have gained popularity in the production of gap waveguides. These techniques include die-sink electric discharge Machining (EDM), 3D printing, plastic injection molding, and micromachining [39]–[43]. By employing these alternative manufacturing methods, the pressure associated with expensive fabrication and precise mechanical assembly of gap waveguide components at the mmWave frequency band can be alleviated.

1.4 Thesis Outline

The main focus of this thesis is to investigate the advancements in automotive radar front-ends based on gap waveguide technology. The research is centered around two main aspects:

1. Firstly, the integration of radar chips with waveguide antennas is explored, with a particular emphasis on the development of waveguide to microstrip transitions. Furthermore, the thesis explores transceivers that utilize advanced packaging techniques, aiming to facilitate easy integration with waveguide antennas.

2. Secondly, the thesis explores the design of gap waveguide antennas with high efficiency, targeting advanced radar systems such as imaging radars and polarimetric radars.

The thesis is structured into two parts:

1. The first part consists of three chapters. Chapter one provides a concise introduction to the background of the thesis work, setting the context for the research. Chapter two focuses on the integration of radar chips with antennas, emphasizing advanced packaging techniques based on gap waveguide technology. Chapter three of the thesis is dedicated to the exploration of antenna designs specifically developed for advanced automotive radar front-ends, with a primary focus on dual circularly polarized antennas utilized in polarimetric radar systems. Additional chapters provide a summary of the papers included in the thesis and explore future possibilities in the field.

2. The second part of the thesis contains the author's contributions in the form of academic research papers. These papers showcase the original research conducted by the author and contribute to the overall body of knowledge in the field of automotive radar front-end advancements.

Integration of radar chips with antennas

2.1 State-of-the-art radar transceivers

Currently, the majority of radar sensing systems employ highly integrated system-in-package (SiP) components that incorporate multiple transmitters (TX) and receivers (RX) featuring a broad range of functionalities, spanning from radio frequency (RF) front-end operations to intermediate frequency (IF) signal processing. As an illustrative example, Fig. 2.1 presents a functional block diagram of the transceiver TI AWR2243 [44]. The transceiver incorporates a comprehensive range of components within its architecture. In addition to RF front-end elements like low-noise amplifiers (LNA), power amplifiers (PA), mixers, and others, it also includes phase-locked loops (PLL) and analog-to-digital converters (ADC). In more advanced designs, microcontroller units (MCU) or digital signal processor (DSP) blocks are further integrated to facilitate signal processing tasks [45]. A comparative analysis of multiple off-the-shelf radar transceivers operating within the frequency range of 76-81 GHz is provided in Table 2.1.

Embedded wafer level ball grid array (eWLB) packaging technique is widely adopted for highly integrated radar transceivers. Fig. 2.2 provides a rep-
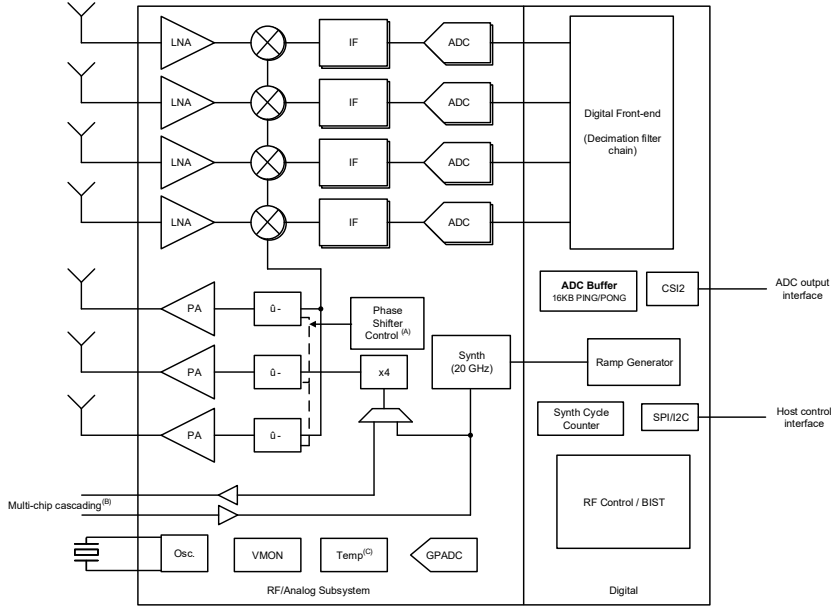
Figure 2.1: Functional block diagram of TI AWR2243 radar transceiver [44].

resentative cross-sectional view of the technique [46]. The view reveals a multi-layered structure, with integrated circuits mounted on redistribution layers, encapsulated with mold compound, and connected to the external world through solder balls. The utilization of eWLB packaging for automotive radar transceivers presents a range of advantages, including miniaturization, enhanced electrical performance, efficient thermal management, and improved reliability. However, it is essential to thoroughly assess factors such as cost, design complexity, and long-term compatibility to ensure successful integration and deployment in automotive radar systems.

The transceivers with eWLB packaging will be surface mounted on PCB boards. This is commonly referred to as flip-chip assembly, as illustrated in Fig. 2.3. In order to establish a dependable electrical connection between the solder balls and PCB pads, the surface mount process must take into account several crucial factors. These include optimizing the solder paste volume, precise component placement, and appropriate reflow temperature [47].
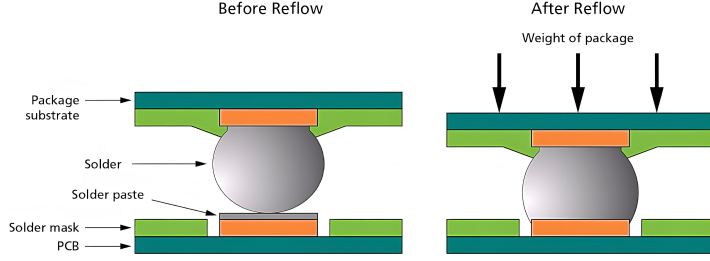
16

Table 2.1: Comparison among off-the-shelf radar transceivers operating at 76-81 GHz.

Transceiver	TX Qty.	RX Qty.	Noise Figure (dB)	Transmit Power (dBm)	Manufacturer
TEF82XX	3	4	11.5	13.5	NXP
TEF810X	3	4	12	12	NXP
AWR1243	3	4	14	12	TI
AWR2243	3	4	12	13	TI
RXS816xPL	3	4	$\sim$	$\sim$	Infineon
RXS8156PLA	2	4	$\sim$	$\sim$	Infineon
CAL77A4T8R	4	8	12	13	Calterah
CAL77A2T4R	2	4	12	13	Calterah
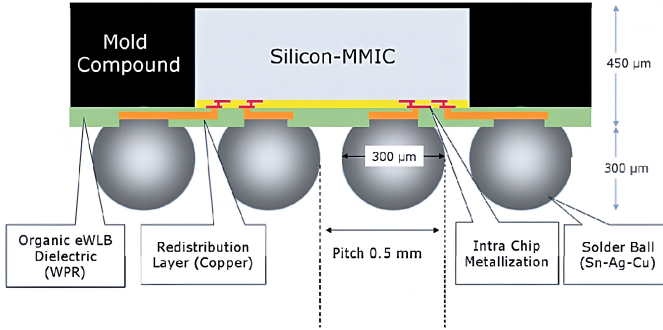
Figure 2.2: Cross-sectional view of an eWLB package [46].

In cutting-edge radar transceivers, the integration of antennas with antenna on package (AoP) technology, referred to as antenna in package (AiP) as well, has reached an advanced stage [48], [49]. AoP technology involves the direct integration of antennas onto the electronic package of the transceiver. Within the context of PCB-based integration, which will be addressed in the forthcoming section, the utilization of AoP technology eliminates the necessity for

Before Reflow

After Reflow

Weight of package

Package substrate

Solder

Solder paste

Solder mask

PCB

Figure 2.3: Surface mount process of the BGA components [47].

a high-frequency substrate material. This elimination results in various benefits, including cost reduction, simplified manufacturing processes, and board space reduction [50]. Nevertheless, it is important to acknowledge that AoP technology also presents certain inherent disadvantages that must be taken into account. These drawbacks include limitations on antenna size due to the compact nature of the package, challenges related to thermal management, difficulties associated with repair or replacement of the integrated antennas, and poor antenna radiation efficiency, among others. These factors need to be thoroughly considered and addressed to ensure optimal performance and reliability of the system.

## 2.2 Integration of radar transceivers with PCB antennas

PCB-based integration stands as the most highly sought-after technique for integrating automotive radar sensors. One of the primary reasons for this preference is the utilization of flip-chip assembly for radar transceivers with BGA packaging, enabling seamless integration with PCB components, including PCB antennas. This approach facilitates efficient integration of the radar system components, ensuring optimal functionalities.

As depicted in Fig. 2.4, an off-the-shelf radar sensor is illustrated with exploded 3D structures. Typically, a radar sensor comprises a housing frame with connectors, a DSP board responsible for signal processing, a shielding metal layer ensuring electromagnetic compatibility, an RF board facilitating

Figure 2.4: Exploded view of the Bosch RADAR sensor [51].

integration of radar transceivers with on-board antennas, and a radome cover.
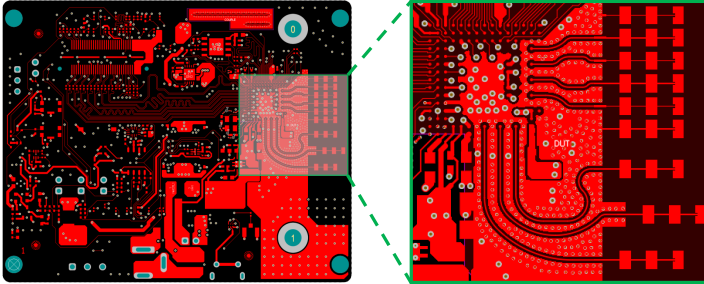
Figure 2.5: PCB layout of TI AWR2243 evaluation module [52].

The transition from eWLB solder balls to PCB antennas, typically in the form of microstrip patch arrays, is a relatively straightforward process, as de-

picted in Fig. 2.5. The solder balls are directly mounted onto grounded coplanar waveguides (GCPW). GCPW is an effective transmission line structure that minimizes coupling between adjacent transmission lines. The presence of grounded vias aids in suppressing parasitic substrate modes. Transitions from GCPW to microstrip lines are achieved using quarter-wavelength transformers.

## 2.3 Integration of radar transceivers with waveguide antennas

The utilization of waveguide antennas is experiencing a notable surge of interest in advanced antenna systems for automotive radar applications. This growing attention is due to the unique characteristics offered by waveguide antennas, such as high power handling capabilities, low loss and wide bandwidth. Waveguide antennas hold significant promise in terms of improving overall performance and enabling advanced beam-forming techniques.

The integration of waveguide antennas with radar transceivers has been investigated in various research studies. In particular, reference [53] presents a simultaneous multi-mode imaging radar system that incorporates a complex antenna system using conventional rectangular waveguide slot arrays. To achieve a lightweight design, the waveguide slot arrays are fabricated using plastic milling techniques. Assembly of the imaging radar system is depicted in Fig. 2.6a. Notably, the waveguide antennas are positioned on top of the RF boards, providing shielding for the active circuits. This design approach allows for a compact stacked configuration, optimizing the use of space within the system. The imaging radar integrates four radar transceivers, which are mounted on an RF board, as illustrated in Fig 2.6b. A crucial aspect of the integration process is the transition from the on-board planar transmission line to the vertically connected waveguide. Proper design and implementation of this transition are essential to minimize losses of the integration. Generally, these types of transitions are classified as broadside E-plane transitions and longitudinal H-plane transitions, as depicted in Fig. 2.7 [54].

Notably, in reference [55], two additional designs of waveguide-to-microstrip transitions are introduced, as depicted in Fig. 2.8. These transitions are specifically designed for operation in the frequency range of 76 to 81 GHz, making them suitable for automotive radar applications. In these designs, the
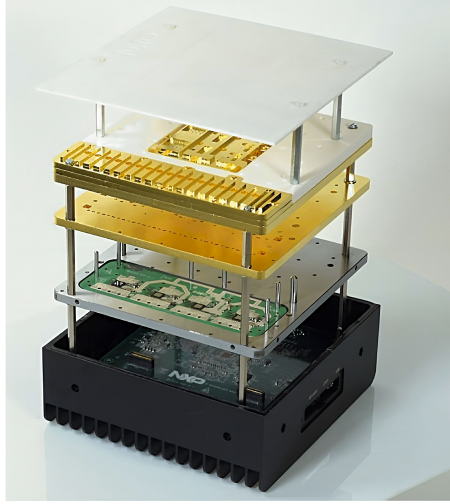
(a)
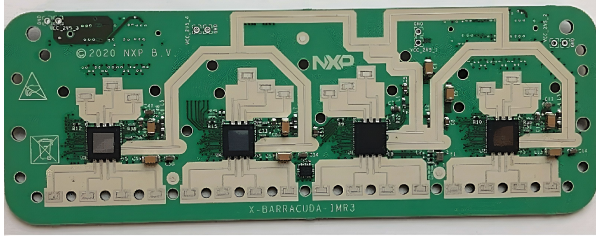
(b)

Figure 2.6: Simultaneous multi-mode automotive imaging radar system using waveguide slot arrays: (a) assembly of the system, (b) RF board integrated with 4 radar transceivers [53].

patch probes are deliberately positioned off the central line in order to generate the desired waveguide modes. Additionally, an elevated ground plane is utilized, which includes metalized vias to prevent any leakage of the electromagnetic field through the substrate. One of the configurations employs a waveguide iris, which helps in achieving a broader bandwidth compared to the other design. It is worth mentioning that both of these transition designs can be implemented effectively on a single-layer printed circuit board (PCB).

(a)   **(b)**
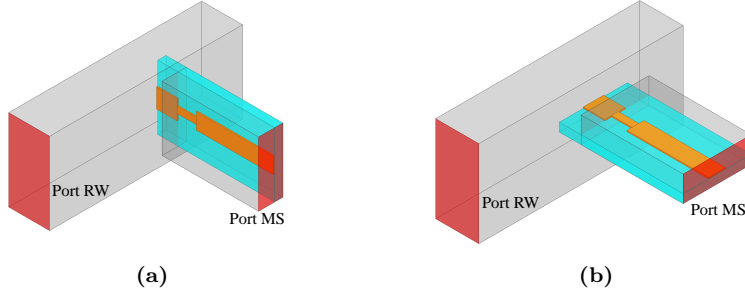
Figure 2.7: (a) broadside E-plane transition from microstrip to waveguide, (b) longitudinal H-plane transition from microstrip to waveguide [54].


(a)   (b)
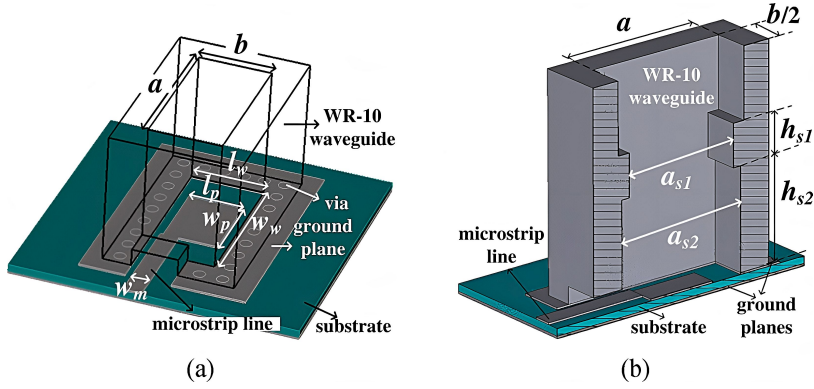
Figure 2.8: 3-D structures of the proposed vertical transitions: (a) without the waveguide iris, (b) with the waveguide iris [55].

Given the presence of differential RF ports in certain off-the-shelf radar transceivers [57], reference [56] presents an intriguing design that focuses on the transition from a differential transmission line to a waveguide, as depicted in Fig. 2.9. The waveguide houses a differential microstrip patch antenna (DMPA) that functions as the radiation element. This antenna consists of a main patch, a short-end parasitic patch, and a matching network. The incorporation of the short-end parasitic patch leads to a significant enhancement in the bandwidth of differential mode signals, while concurrently providing strong suppression of common mode signal transmission.
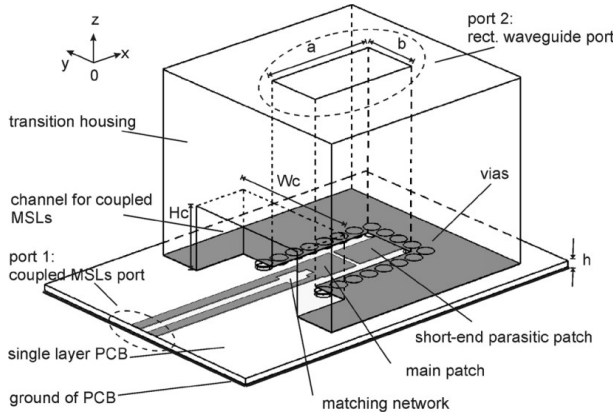
Figure 2.9: Structure of vertical transition between rectangular waveguide and differential line as proposed in [56].

2.4 Integration of automotive radar front-end based on gap waveguide technology
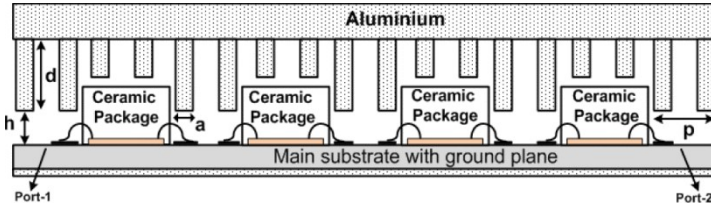
Figure 2.10: Gap waveguide packaging model for an amplifier chain [58].

In addition to its growing utilization in multi-layer waveguide antenna design, gap waveguide technology has been recognized for its active circuits packaging capabilities, which offer improved isolation between adjacent components, as depicted in Fig. 2.10 [58]. The periodic pin textures effectively mitigates electromagnetic field leakage through the air gap. Importantly, this approach does not require electrical contact between the layers, further simplifying the design and assembly process.

This packaging technique has been employed in the design of waveguide-to-

(a)

(b)
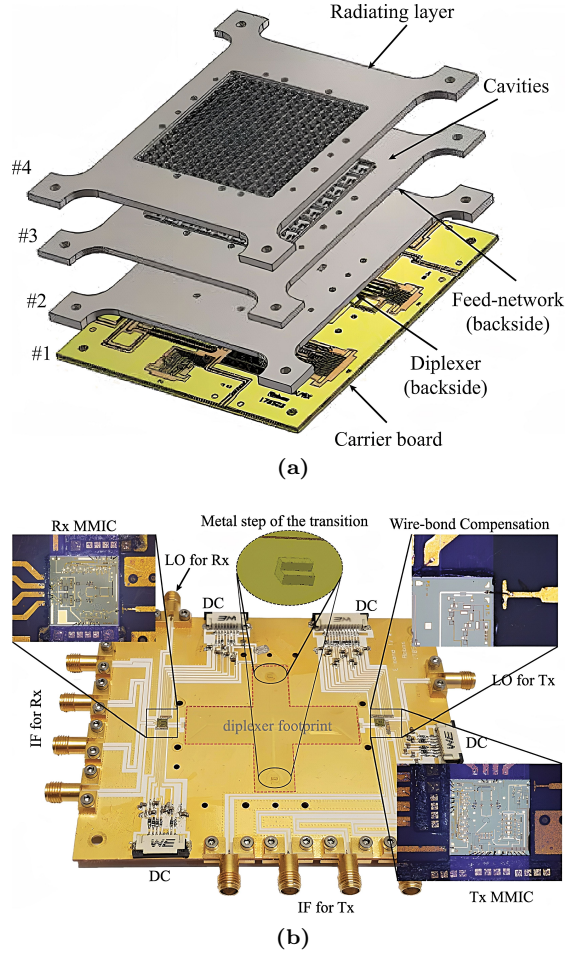
Figure 2.11: (a) Configuration of the proposed RF front-end, (b) RF board integrated with transitions and MMICs [37].

microstrip transitions for the integration of waveguide-based RF front-ends. Reference [37] presents an example of an RF front-end designed for high data rate communications in the E band, employing gap waveguide technologies. This example serves as an inspiring reference for the integration of waveguide-based automotive radar front-ends. The design comprises a 16×16 gap waveg-
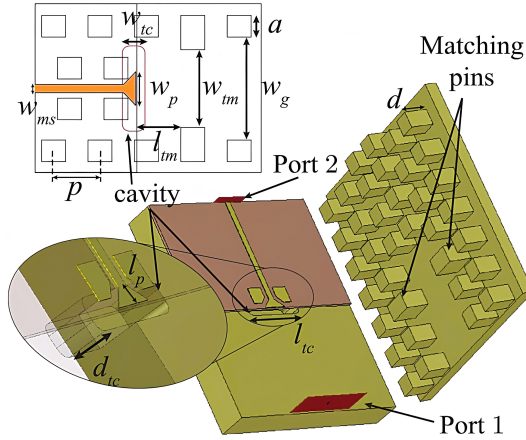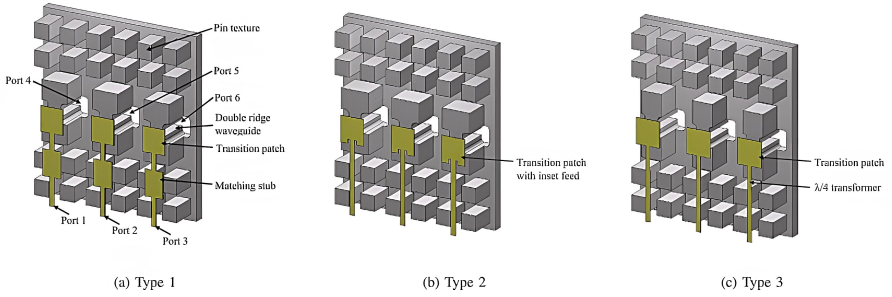
Figure 2.12: Configuration of the proposed microstrip-to-waveguide inline transition [37].

uide slot array equipped with an input diplexer, positioned on the top of the RF board, as depicted in Fig. 2.11a. The integration of RX and TX MMICs with the RF board is achieved through bond-wire connections as illustrated in Fig. 2.11b. The waveguide antenna is seamlessly integrated with the RF board via inline transitions from microstrip to groove gap waveguide as depicted in Fig. 2.12. The inline transition can be categorized as a broadside E-plane transition. A back-short cavity is employed beneath the microstrip probe. To attain broadband matching, a pair of closely positioned parasitic patches are incorporated near the probe. Two metallic pins that positioned quarter wavelength away from the E-plane probe are extended into the waveguide channel in order to improve the impedance matching of the transition.

However, the implementation of inline transitions requires the placement of both the MMIC and gap waveguide transmission line in the same layer. Consequently, this configuration restricts the available space for routing bias signals and LO/IF signals, leading to limitations in signal routing capabilities. In contrast to the inline transitions, as discussed in the preceding section, vertical transitions offer greater compactness and flexibility in the integration of multiple active components.

Notably, the previous analysis of vertical transitions in [55], [56] has revealed that a considerable portion of board space is occupied by metalized vias. Fur-

thermore, the assembly process requires establishing electrical contact between the waveguide block and an elevated ground plane. Consequently, there exists a significant risk of electromagnetic (EM) field leakage through potential air gaps, particularly at the mmWave frequency band. On the contrary, packaging techniques utilizing gap waveguides offer a compelling alternative for vertical transition designs. These techniques involve non-galvanic contact between the layers, which effectively mitigates the risk of field leakage through air gaps.

(a) Type 1 (b) Type 2 (c) Type 3

Figure 2.13: Structures of the proposed microstrip to double ridge transitions. In these figures, substrate and ground layer of microstrip lines are not shown [59].
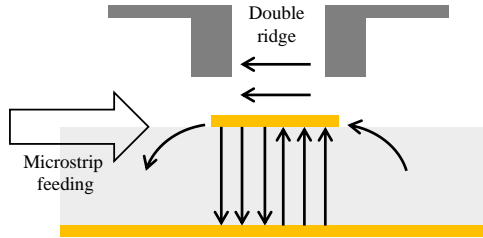
Figure 2.14: Electric field distribution surround the patch.

In the work presented in [59], three vertical transitions from microstrip to double ridge waveguide are proposed, as depicted in Fig. 2.13. They are classified as broadside E-plane transitions, primarily designed to operate at the 28 GHz frequency band. However, due to their inherent design characteristics,

they can be easily scaled for use in the 77 GHz frequency band. They are realized by employing microstrip patches with double ridge metal posts positioned on top. The fringe fields generated by the patches enable vertical coupling to the double ridge, as illustrated in Fig. 2.14. Notably, the need for metalized vias is eliminated due to the periodic pins that effectively prevent the field from propagating through the substrate. Despite their close proximity, these transitions achieve remarkable isolation, which can be attributed to the gap waveguide packaging. Moreover, these transitions can be implemented on a single-layer PCB.
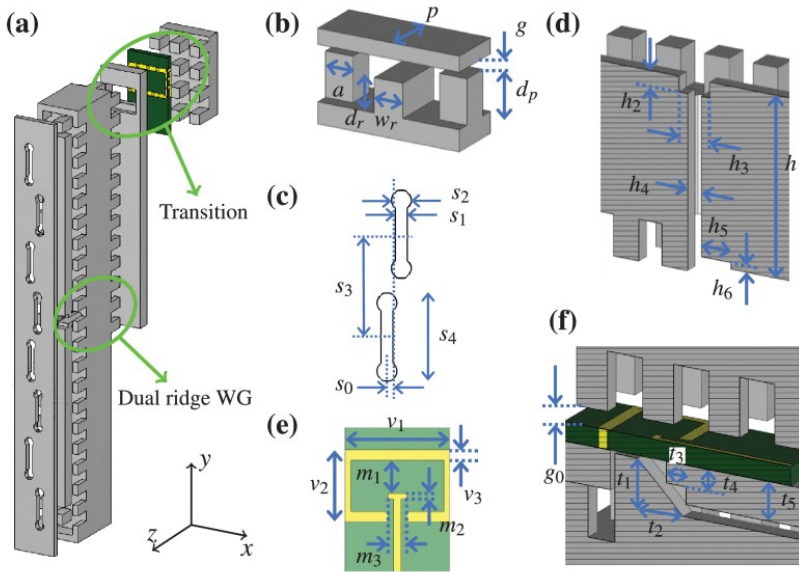
Figure 2.15: (a) Exploded view of the design sketch of subarray integrated with the transition. (b) Ridge GW unit cell, where a ridge is embedded within a pin texture. (c) Layout of two slots of slot layer. The rest of the slots are similar. (d) yz -plane cross section sketch of the dual ridge waveguide. (e) Layout of the microstrip probe is used in the transition. (f) yz -plane cross section of microstrip line to ridge GW line transition [60].

In reference [60], an additional example of a vertical waveguide-to-microstrip transition is discussed, which is based on the concept of gap waveguide. This

transition is specifically designed for a phased array system operating at 28 GHz but also serves as an inspiring design for potential applications at 77 GHz. The transition, classified as a broadside E-plane transition, utilizes the pin texture of the gap waveguide to effectively block the propagation of the electromagnetic field in the backward direction, as depicte in Fig. 2.15. An SIW cavity with vias on board is connected to the waveguide port, which is then followed by a transition to the distribution RGW. It is important to note that while this design cannot completely eliminate electrical contact, the metal pieces of the antenna serve the purpose of heat dissipation and contribute to the temperature stability of the system.

2.5 Contributions of the thesis

### Research on vertical gap waveguide-to-microstrip transitions

The previous publications primarily concentrate on vertical gap waveguide to microstrip transitions operating at lower frequency bands, with limited validation through active measurements. In this thesis, two vertical transitions are introduced, designed specifically for the integration of RGW with MMICs, operating at the 77 GHz frequency band. In addition, the transitions have undergone comprehensive verification through both passive and active measurements.

The first vertical transition utilizes a rectangular microstrip patch to couple the signal to the RGW, as dipicted in Fig. 2.16. Measurement results of this transition in a back-to-back structure demonstrate that the reflection coefficient is better than -10 dB from 75 to 83 GHz, as depicted in Fig. 2.17. The insertion loss for this exclusive transition over the frequency band is derived to be in the range of 0.65 to 0.85 dB based on the measurement results. The second vertical transition utilizes a microstrip probe with a ground slot as depicted in Fig. 2.18. Measurement results of this transition in a back-to-back structure show that the reflection coefficient is better than -10 dB from 69 to 86 GHz, as depicted in Fig. 2.19. The insertion loss for this exclusive transition over the frequency band is derived to be in the range of 0.65 to 1 dB based on the measurement results. Please notice that the conclusions regarding the losses of the transition are not directly obtained from the measurements but are derived with the assistance of simulated results. In principle, more

accurate results could be obtained through the utilization of dedicated Thru-Reflect-Line (TRL) calibration kits, as suggested in reference [61], [62]. Please refer to the research details in Appendix **Paper A** for further information.
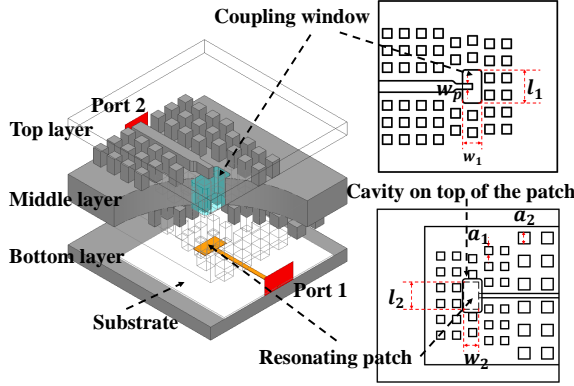
Figure 2.16: Vertical transition A between packaged microstrip line and RGW. (a_1 = 0.55 mm, a_2 = 0.8 mm, l_1 = 2.33 mm, w_1 = 1.34 mm, l_2 = 1.89 mm, w_2 = 1.04 mm)

(a) S_{11}

(b) S_{21}
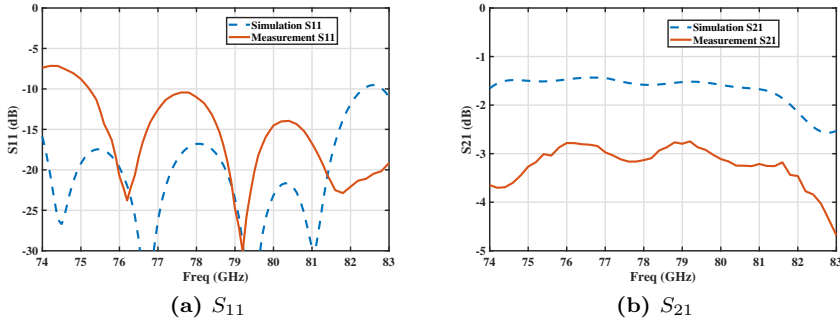
Figure 2.17: Simulated and measured results of transition A implemented in a back-to-back structure.
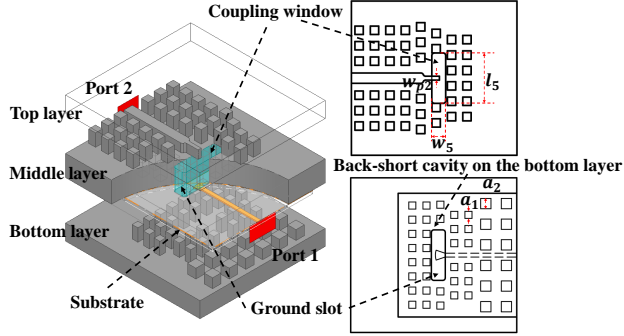
Figure 2.18: Vertical transition B between packaged microstrip and RGW. ($w_5 = 1.08$ mm, $l_5 = 3.92$ mm, $w_{p2} = 0.3$ mm)

(a) S_{11}

(b) S_{21}

Figure 2.19: Simulated and measured results of transition B implemented in a back-to-back structure.
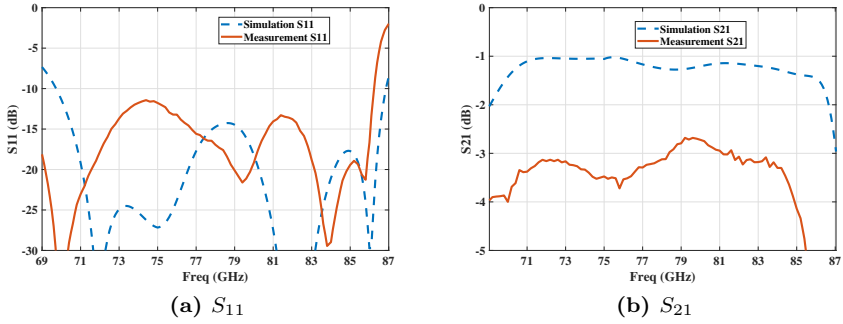
Research on gap waveguide based polarimetric radar front-ends

Currently, there are limited publications focusing on waveguide-based automotive radar front-ends, particularly those supported by measurement verification. This thesis addresses this research gap by presenting the development of a comprehensive polarimetric radar sensor. The RF front-end of the sensor adopts a multi-layer configuration based on gap waveguide technology. To enable seamless integration of the waveguide front-end with RF boards, ver-
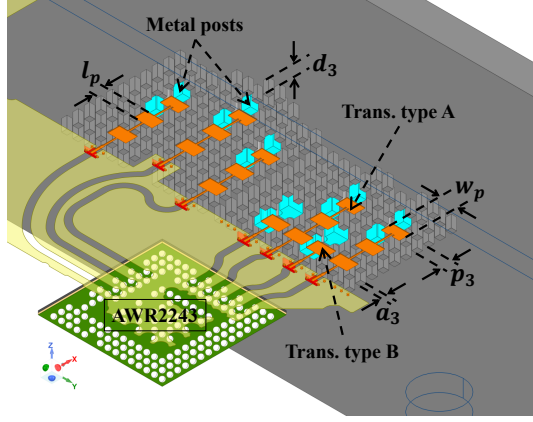
(a)
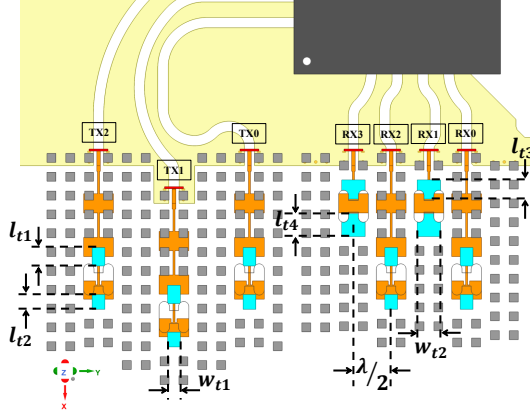
(b)

Figure 2.20: a) Non-galvanic waveguide-to-microstrip transitions based on gap-waveguide technology. b) Top view.

tical waveguide-to-microstrip transitions utilizing gap waveguide packaging techniques are employed. A visual depiction of the transition can be found in Fig. 2.20. The insertion losses of the transitions are determined through comparative measurements conducted with a reference radar system that features identical electronic circuitry with the proposed polarimetric sensor. For

further in-depth information, please refer to the research details provided in Appendix **Paper D**.

Research on imaging radar front-ends based on advanced radar transceivers with launcher-in-package technology

In this theis, a highly integrated radar transceiver utilizing launcher-in-package (LiP) technology is introduced. The transceiver is equipped with four receivers and three transmitters. Notably, the transceiver incorporates RF ports with waveguide interfaces, facilitating direct integration with waveguide antennas. To ensure reliable interconnectivity between the transceivers and waveguide antennas, a novel approach utilizing gapwaveguide packaging technology is proposed, as depicted in Fig. 2.21. This approach enables non-galvanic contact between the transceivers and waveguide antennas, ensuring robust signal transmission. For further in-depth information, please refer to the research details provided in Appendix **Paper C**.
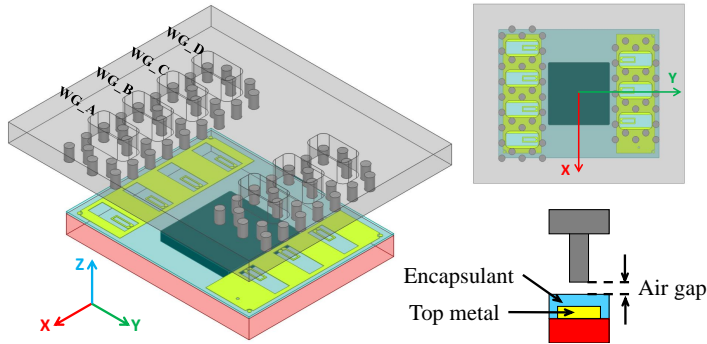
**Figure 2.21:** Compact gapwaveguide interconnects for the LiP transceivers.

Antenna Designs of Automotive Radar Front-ends

3.1 Antenna designs based on PCB technology

Chapter 2 of the thesis highlights the significance of eWLB technology, which offers the advantage of flip-chip assembly for transceivers. This flip-chip assembly approach is particularly beneficial for applications based on printed circuit boards (PCBs). Consequently, it logically follows that PCB antennas have become the most commonly employed antennas integrated with the transceivers.

Microstrip patch antennas have gained significant popularity as on-board antennas primarily because of their straightforward integration with PCBs. Their planar structure and compatibility with PCB fabrication processes make them easily integrated into the board layout. In particular, series-fed microstrip patch arrays have been extensively investigated. This is primarily attributed to the ease of implementing compact feeding networks within series-fed configurations. Fig. 3.1 displays a selection of off-the-shelf automotive radar sensors available in the market, which utilize series-fed patch arrays [63]–[66]. In the design of series-fed patch arrays, a common practice is to maintain a distance between adjacent patches that is approximately equal to
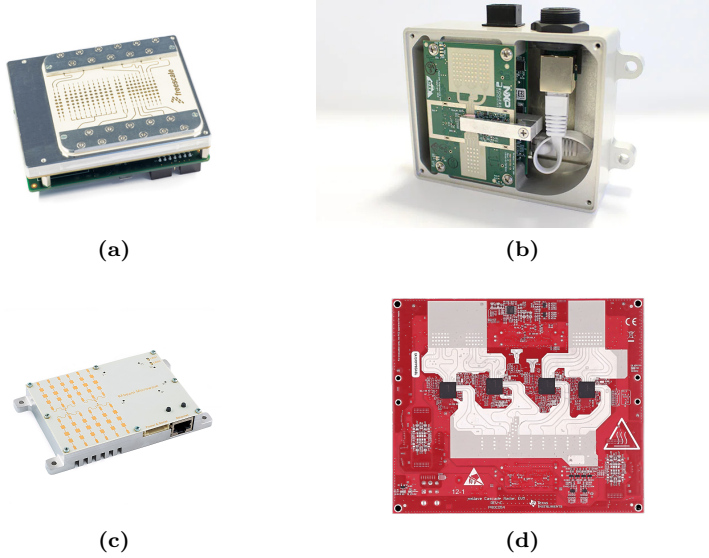
Figure 3.1: Radar sensors on the markets: (a) 76-77 GHz radar sensor with 4 TXs and 6 RXs [63], (b) 77 GHz radar sensor with 3 TXs and 4 RXs [64], (c) 24GHz FMCW radar sensor with 1 TX and 3 RXs [65], (d) 77 GHz mmWave cascade imaging radar RF evaluation module with 12 TXs and 16 RXs [66].

one guided wavelength. The width of the patches is then optimized to achieve a desired excitation distribution, while the length of the patches is typically set to half of the guided wavelength. In addition to the conventional design of linearly polarized series-fed patch arrays, alternative configurations such as differential patch arrays and comb-line patch arrays have been explored as well, as depicted in Fig. 3.2 [67], [68]. These variations offer alternative approaches to address specific application requirements.

In spite of the aforementioned benefits, for PCB antennas, it is crucial to employ low-loss and cost-effective dielectric materials. Furthermore, factors such as thermal expansion and moisture absorption of the dielectrics can influence the stability of radar systems. To mitigate issues related to lossy routing of feeding lines, transceivers are commonly placed in close proximity to PCB antennas. However, this arrangement can give rise to challenges such as trans-
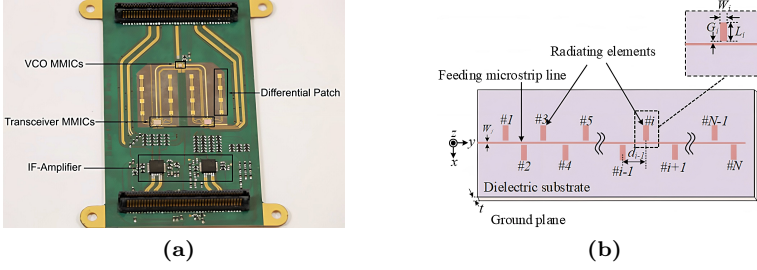
Figure 3.2: Configuration of the proposed (a) differential patch array [67] and (b) comb-line patch array [68].

mitting/receiving isolation, electromagnetic compatibility of the transceiver, and interference on the radiation pattern, among others. Furthermore, in complex antenna systems, such as the imaging radar system depicted in Fig. 3.1d, where numerous antennas are employed, the use of PCB antennas, which commonly employ a single-layer structure to minimize costs, poses limitations in terms of their flexibility for routing feeding lines and positioning antenna elements. As a result, the requirement to allocate a significant board area for antenna accommodation, along with the deployment of complicated routing lines, leads to a large form factor and severe substrate loss.
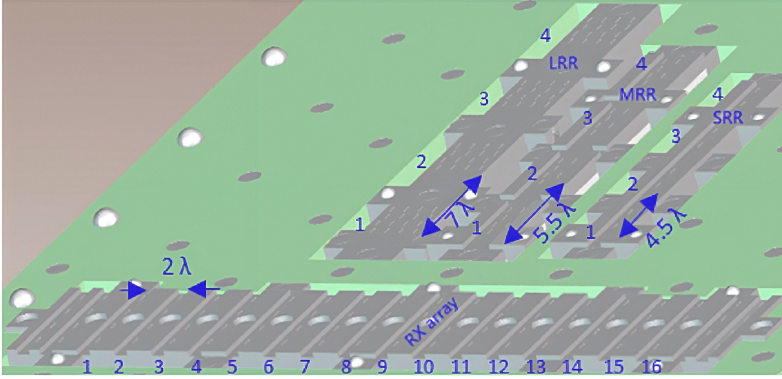
Figure 3.3: Simultaneous multi-mode automotive imaging radar system using waveguide slot arrays. [53].

3.2 Waveguide antennas for automotive radar front-ends

As outlined in Chapter 2, waveguide antennas possess distinctive attributes, including high power handling capabilities, low loss, and wide bandwidth. Consequently, these characteristics have gained substantial attention for their deployment in advanced automotive radar front-ends.
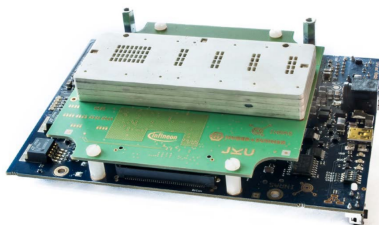
(a)
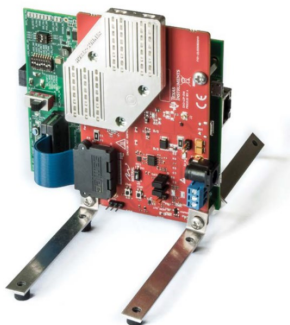
(b)

Figure 3.4: a) Demonstrator radar sensor developed by HUBER+SUHNER with Infineon. b) Mid-range demonstrator radar sensor developed by HUBER+SUHNER with Texas Instruments [69].

Recently, conventional waveguide slot arrays have emerged as a viable choice for advanced imaging radar front-ends. A notable example can be found in the work presented in [53]. In this study, a simultaneous multi-mode imaging

radar system is demonstrated, employing waveguide slot arrays. The system incorporates four radar transceivers, each equipped with three transmitters (TXs) and four receivers (RXs), enabling high angular resolution in both azimuth (AZ) and elevation (EL). The proposed antenna system utilizes complex Multiple-Input Multiple-Output (MIMO) configurations. Specifically, 16 RX antennas are positioned side-by-side, while the 12 TX antennas are categorized based on different operating modes. The antennas are implemented with high efficiency through the utilization of waveguide slot arrays, as depicted in Fig. 3.3. Moreover, the multilayer structure of the arrays facilitates the design approach with a remarkable degree of flexibility.

An additional noteworthy aspect arising from the aforementioned example is the employment of a low-cost plastic milling technique in the manufacturing process. Conventionally, waveguide slot arrays were fabricated using computer numerical control (CNC) milling techniques, which tend to be both time-consuming and cost-prohibitive. However, recent advancements in fabrication technologies, such as 3D printing and metallic plastics, have facilitated the development of cost-effective waveguide components with high efficiency, specifically within the mmWave frequency band. Reference [69] introduced several antenna designs fabricated by using metallic plastic, as depicted in Fig. 3.4.

3.3 Antenna designs for polarimetric radar systems

To achieve a compact and cost-effective antenna system with polarimetric capability, the utilization of dual-polarized microstrip patch arrays has been investigated [11], [70]. In the study presented by [11], radar systems employing left-hand circularly polarized transmitters (TXs) and dual linearly polarized receivers (RXs) are discussed. The antennas are based on square patch elements with series-parallel feeding networks and can be implemented on a single-layer printed circuit board (PCB), as depicted in Fig. 3.5a. The patch elements are inclined at an angle of 45° to achieve orthogonal linear polarizations. Extensive optimization has been conducted on the square patches to minimize side-lobe levels. Furthermore, a circularly polarized TX antenna is realized by combining the excitation ports that related to both linear polarization with a 90° hybrid network, as illustrated in Fig. 3.5b.

The topic of fully polarimetric automotive radar sensors based on waveguide

(a)

(b)
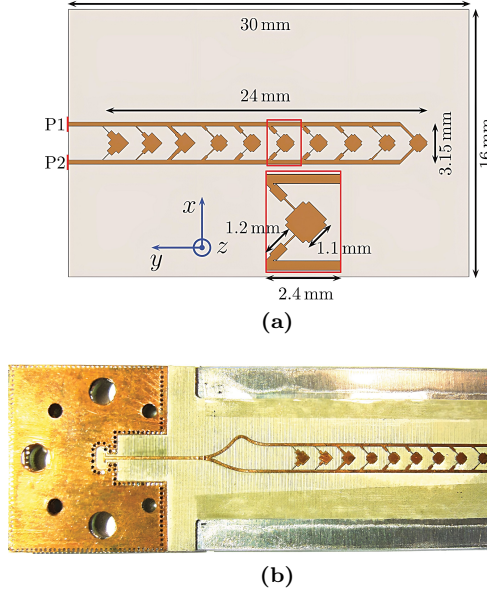
Figure 3.5: Configuration of the proposed patch array (a) dual linearly polarized
and (b) left hand circularly polarized [11].

antennas is explored in detail in [16]. Fig. 3.6 illustrates the proposed po-
larimetric MIMO systems utilizing sectoral waveguide horn antennas. Specif-
ically, E-plane sectoral horns are employed to achieve vertical polarization,
while H-plane sectoral horns are used for horizontal polarization. Sectoral
horn antennas are well-suited for automotive radar applications due to their
ability to provide broad azimuth patterns and narrow elevation patterns. The
systems described in the papers operate based on time division multiplexing
(TDM) operation. Configuration A results in a MIMO virtual array with an-
gular ambiguities while configuration B represents an improved design that
addresses these ambiguities. Although sector horn antennas feature high po-
larization isolation, they are not well-suited for low-profile designs and lack
scalability in high-gain scenarios, such as long-range radar applications.

Dual circularly polarized waveguide antennas are also investigated for po-
larimetric radar applications. Reference [71] introduces a polarimetric radar
sensor that integrates 6 left-hand circularly polarized (LHCP) transmitting

(a)

(b)
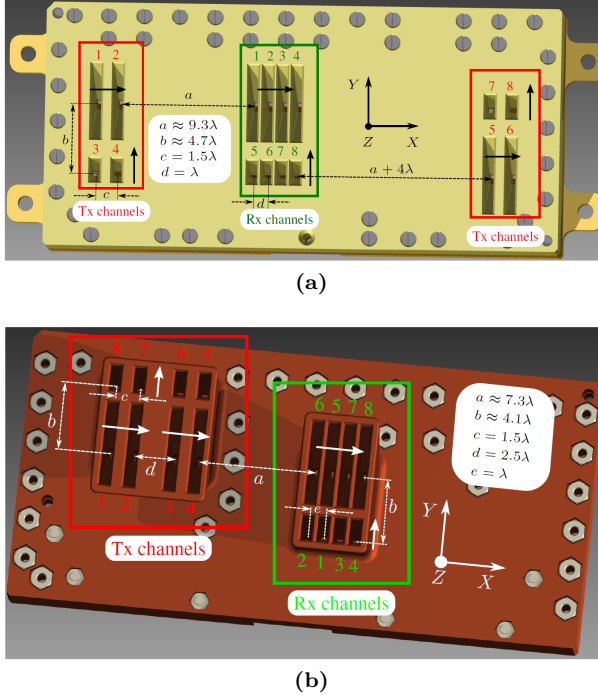
Figure 3.6: Proposed dual-polarized MIMO waveguide antenna: (a) configuration A, (b) configuration B [16].

antennas and 16 dual circularly polarized receiving antennas, as illustrated in Fig. 3.7. The receiving antennas consists of 16 linear arrays arranged in azimuth. Each linear array is composed of of 8 dual circularly polarized corrugated horns. These horns are designed with classic septum polarizers to generate dual circular polarizations. Additionally, the horns are equipped with corporate feeding networks, which are implemented using T-junctions in a vertical configuration. To accommodate the size constraints of the horns, the receiving antennas are spaced apart by one wavelength, while the transmitting antennas are spaced apart by 1.5 wavelengths. By utilizing TDM MIMO operation, a virtual array with a half wavelength spacing is achieved. It should be noted that the transmitting antenna array has a lattice configuration of 3×2, enabling the system to perform direction of arrival (DoA) estimation in

both azimuth and elevation.

(a)

(b)
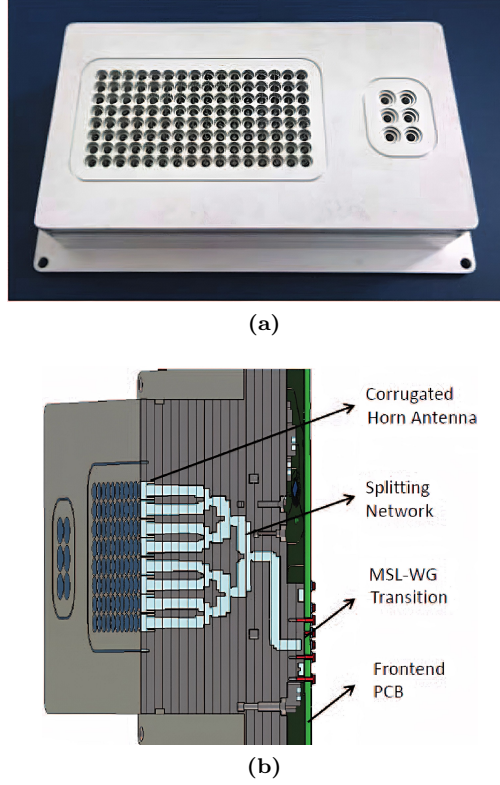
Figure 3.7: Configuration of the proposed dual circularly polarized waveguide array: (a) fully-manufactured prototype, (b) cross section of the waveguide array [71].

Similar to the methodology illustrated in Figure 3.5b, a dual-circularly polarized waveguide antenna can be realized by combining a dual-linearly polarized waveguide antenna with a 90° hybrid network, as studied in [72], although the design is for Ka-band satellite communications. A detailed exploded view of this design is provided in Fig. 3.8. Notably, this design features a shared aperture for dual circular polarization with independent feeding networks on separate layers.

In summary, dual polarized waveguide antennas are considered excellent

Hybrid   V-Pol Layer   H-Pol Layer   Lid
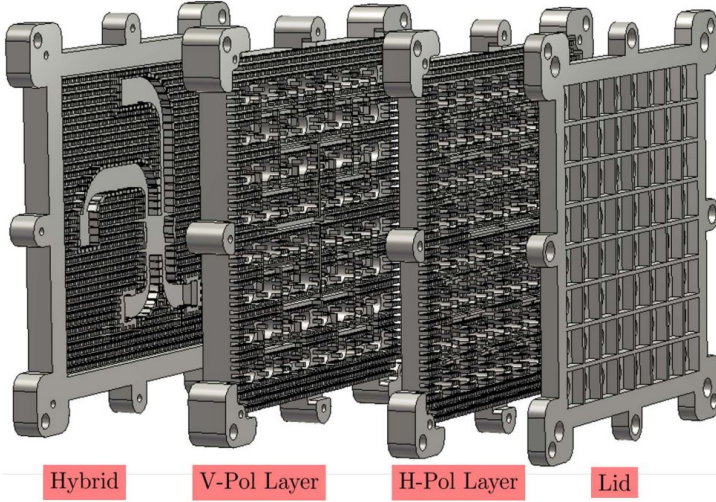
Figure 3.8: Exploded side view of the full antenna [72].

choices for the implementation of advanced polarimetric radar systems. While polarimetric radar systems can utilize either dual linear polarization (LP) or dual circular polarization (CP), the latter offers advantages over the former in terms of mitigating challenges such as multi-path fading and signal degradation [73]. Therefore, there is significant interest in exploring polarimetric radar systems that leverage the capabilities of dual circularly polarized waveguide antennas.

Waveguide polarizers, such as septum polarizers, are commonly employed to generate circularly polarized waves directly. The septum polarizer consists of two rectangular waveguide input ports separated by a septum, as shown in Fig. 3.9. Ports 3 and 4 are overlapped and realized by quadratic waveguides. In an ideal lossless scenario, the septum polarizer can be described by a scattering matrix:

$$[S_{ij}] = \frac{1}{\sqrt{2}} \begin{bmatrix} 0 & 0 & 1 & -j \\ 0 & 0 & -j & 1 \\ 1 & -j & 0 & 0 \\ -j & 1 & 0 & 0 \end{bmatrix} \qquad (3.1)$$

Here, $S_{ij} = V_i^- / V_j^+$ where V_i^- represents the amplitude of the wave leaving port i and V_j^+ represents the amplitude of the wave exciting port j. When port 1 is excited, the electric field at the output can be expressed as:

$$\mathbf{E}_{RHCP} = S_{31}\hat{\mathbf{x}} + S_{41}\hat{\mathbf{y}} = (\hat{\mathbf{x}} - j\hat{\mathbf{y}})/\sqrt{2} \qquad (3.2)$$

This represents RHCP. On the other hand, when port 2 is excited, the electric field at the output is given by:

$$\mathbf{E}_{LHCP} = S_{32}\hat{\mathbf{x}} + S_{42}\hat{\mathbf{y}} = (-j\hat{\mathbf{x}} + \hat{\mathbf{y}})/\sqrt{2} \qquad (3.3)$$

This represents LHCP.
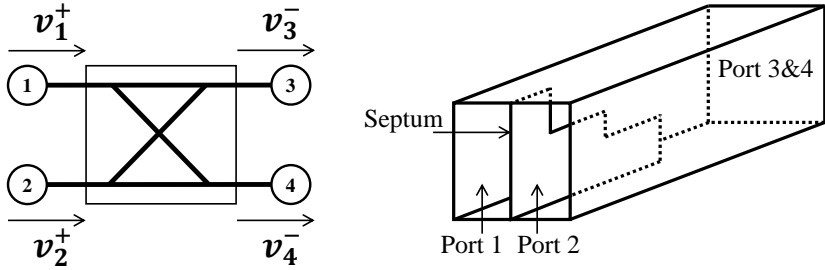
Figure 3.9: Illustration of a four-port septum polarizer.

The use of quadratic waveguide outputs is highly advantageous, especially for feeding circular waveguide horn antennas with dual circular polarization, as highlighted in the reference [74]. The septum polarizer has also been explored in planar array designs, as discussed in reference [75]. However, it is important to note that despite their compact size, septum polarizers pose challenges in terms of fabrication and assembly, particularly at mmWave frequency ranges.

In recent research, the utilization of grooved circular waveguide polarizers has gained attention for the design of dual circularly polarized antennas. Several studies, such as [76]–[79], have focused on investigating this approach. Fig. 3.10 illustrates the concept of grooved circular waveguides, which involve circular waveguides with sector grooves. These grooves can be categorized into different types, such as mono-grooved circular waveguides and double-grooved circular waveguides. Moreover, these configurations can also be considered as circular waveguides with embedded sector ridges, thus referred to as ridged

circular waveguides. Rigorous analytical solutions addressing wave propagation in ridged circular waveguides have been presented in previous studies [80], [81].
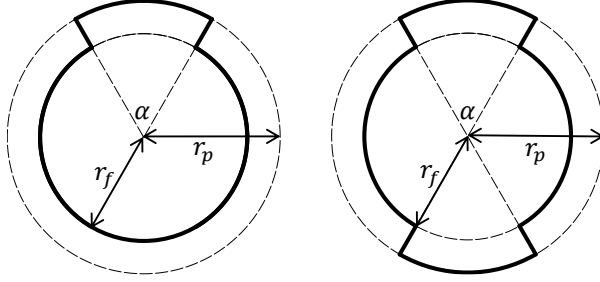
Figure 3.10: Sectional view of (left) mono-grooved circular waveguide and (right) double grooved circular waveguide.

A segment of grooved circular waveguide can serve as a polarizer to generate circularly polarized waves, as depicted in Figure 3.11. When the excitation field at the input is polarized in the Y direction, the dominant TE11 mode inside the circular waveguide (referred to as $\mathbf{E_R}$) can be decomposed into two orthogonal components, $\mathbf{E_{R1}}$ and $\mathbf{E_{R2}}$, with equal amplitudes. As the field propagates through the double-grooved circular waveguide, $\mathbf{E_{R2}}$ experiences a larger propagation radius than $\mathbf{E_{R1}}$. Consequently, a phase difference between the two components arises at the output, given by:

$$\Delta\phi = \phi_1 - \phi_2 = (\beta_1 - \beta_2)L_p \tag{3.4}$$

where

$$\beta_1 = \sqrt{k^2 - (\frac{p'_{11}}{r_f})^2} \tag{3.5}$$

$$\beta_2 = \sqrt{k^2 - (\frac{p'_{11}}{r_p})^2} \tag{3.6}$$

β_1 and β_2 represent the wave numbers of $\mathbf{E_{R1}}$ and $\mathbf{E_{R2}}$, respectively, and L_p denotes the length of the double-grooved circular waveguide section. The parameter p'_{mn} corresponds to the first root of the derivative of the first-order Bessel function. By introducing a 90° delay between $\mathbf{E_{R1}}$ and $\mathbf{E_{R2}}$, the output

field exhibits right-hand circular polarization. Similarly, when the input field is polarized in the X direction, a left-hand circularly polarized wave can be generated if $\mathbf{E_{L2}}$ leads $\mathbf{E_{L1}}$ by $90°$ at the output.
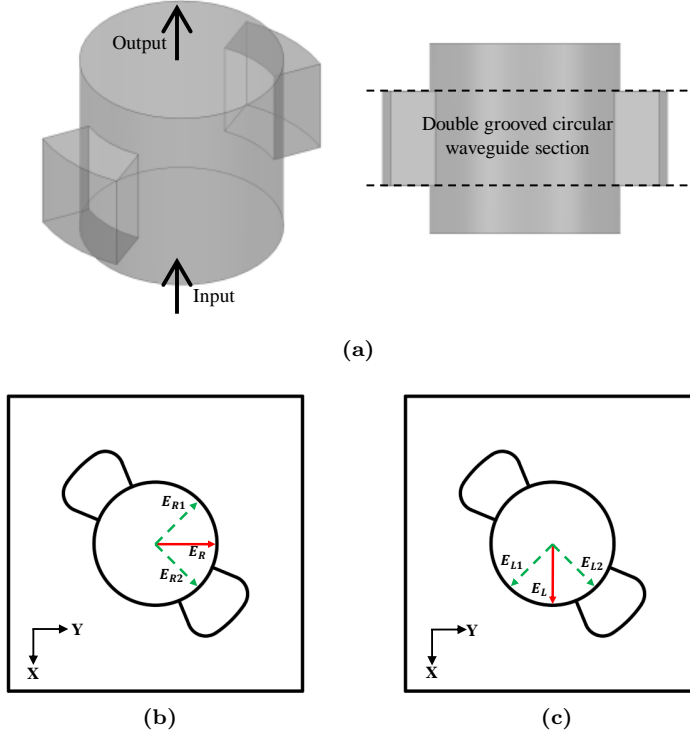
Figure 3.11: Illustration of double grooved circular waveguide polarizer.

In [77], the authors discuss polarizers based on mono-grooved circular waveguides. However, compared to double-grooved circular waveguide polarizers, mono-grooves exhibit larger dimensions and their asymmetric configurations can adversely affect the bandwidth of the polarizer.

3.4 Contributions of the thesis

Automotive imaging radar antennas based on gap waveguide technology

As discussed in Section 3.1, complex imaging radar antennas that consist of a large number of antenna elements encounter numerous challenges when implemented using PCB technology. This thesis presents the development of an automotive imaging radar antenna utilizing gapwaveguide technology, as depicted in Fig. 3.12. The antenna design incorporates designated antenna elements implemented as slot arrays utilizing center-fed ridge gapwaveguides. The overall structure of the imaging radar antenna consists of three layers: a top radiating slot layer, a middle distribution layer, and a bottom interconnect layer. The interconnect layer is specifically designed to accommodate four launcher-in-package transceivers, allowing for significant assembly tolerance. Part of the antenna measurement results are depicted in Fig. 3.13. For further in-depth information, please refer to the research details provided in Appendix **Paper C**.

Dual-circularly polarized array antenna based on gap waveguide utilizing double-grooved circular waveguide polarizer

The utilization of grooved circular waveguide polarizers in an array configuration has been limited due to the complexity of fabrication and size constraints. However, this thesis introduces a novel planar array that incorporates double grooved circular waveguide polarizers, as depicted in Fig. 3.14. The planar array is specifically designed for fixed beam, high gain polarimetric sensing applications. The antenna structure consists of six layers, including three layers dedicated to the feeding networks, one layer for the polarizer, one layer for the back cavity, and another layer for the radiating grid. To facilitate the operation of the array, independent, highly isolated, and compact feeding networks based on gap waveguide technologies are proposed. Measurement results of the antenna's axial ratio is depicted in Fig. 3.15. For a detailed understanding of the design, please refer to the appended **Paper B**.

45
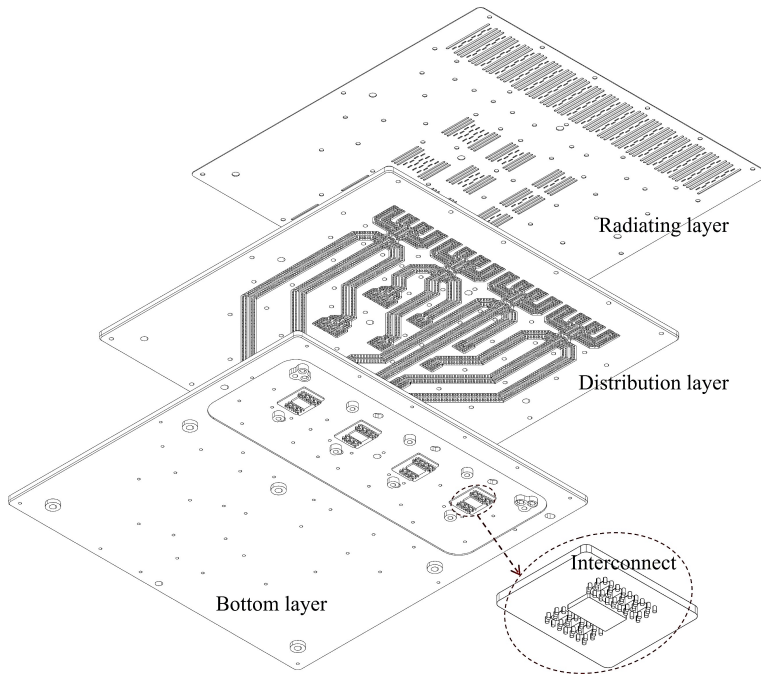
Figure 3.12: Automotive imaging radar aiming for LiP technology.
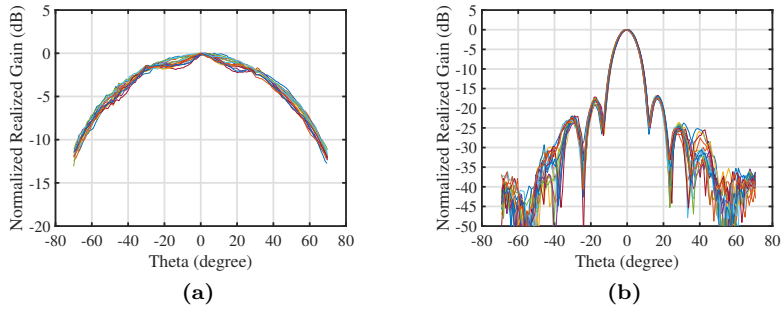
Figure 3.13: Measured radiation patterns of RX slot arrays at 76.5 GHz with all 16 elements plotted together: (a) E-plane, (b) H-plane.
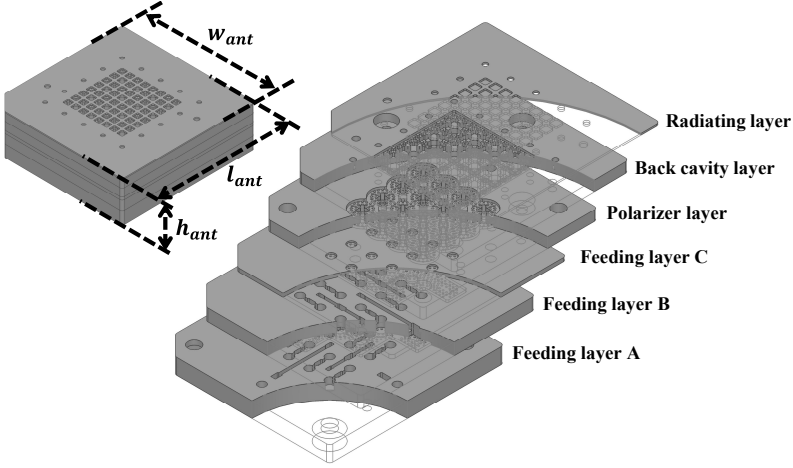
Figure 3.14: Multi-layer structure of the dual-circularly polarized planar array.

Figure 3.15: Simulated and derived axial ratios over frequency of the planar array: (a) RHCP; (b) LHCP.

Antenna designs based on series-fed septum polarizers for polarimetric MIMO radars

In automotive MIMO radar systems, the typical design for an antenna element is a linear array that exhibits a narrow beam width in the EL plane and a broad beam width in the AZ plane. For polarimetric MIMO radars, waveguide dual-CP linear arra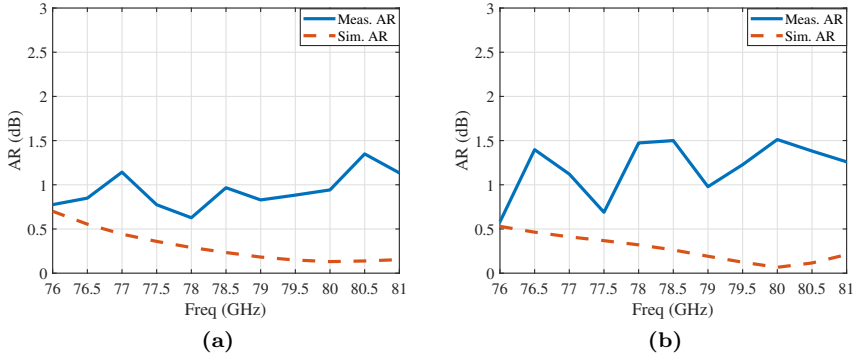ys are considered a promising choice. However, these arrays often utilize corporate feeding networks with a vertical configuration, resulting in a multi-layer design. This multi-layer design poses challenges in achieving low-profile characteristics, as highlighted in [21]. Additionally, the assembly of multiple layers becomes critical, particularly in the millimeter-wave frequency band. In this thesis, antenna designs based on series-fed septum polarizers are presented with low-profile characteristics for polarimetric MIMO radars, as depicted in Fig. 3.16. Gapwaveguide technology is utilized for the implementation of the multi-layer waveguide front-end. Measurement results of the RX antennas' axial ratios are depicted in Fig. 3.17. For further in-depth information, please refer to the research details provided in Appendix **Paper D**.
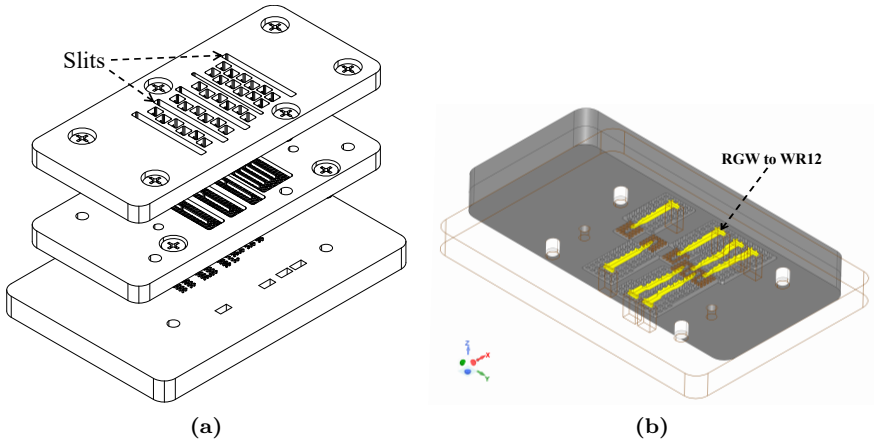
Figure 3.16: a) The proposed multi-layer antenna module. b) Distribution of the antenna elements with vertical transitions to standard WR12 waveguides.

Figure 3.17: Measured axial ratios of the RX antenna elements: a) RX0, b) RX1, in azimuth plane.

CHAPTER 4

Summary of included papers

This chapter provides a summary of the included papers.

4.1 Paper A

Two vertical transitions for integration of RGW with MMICs and one novel packaging structure for integration of IMGW with MMICs have been presented in this chapter. The first vertical transition utilizes rectangular microstrip patch to couple the signal to RGW. Measurement results of the transition in a back-to-back structure show that the reflection coefficient is better than -10 dB from 75 to 83 GHz and the insertion loss for an exclusive transi-

tion over the frequency band is 0.65 to 0.85 dB. The second vertical transition utilizes a microstrip probe with a ground slot. Measurement results of the second transition in a back-to-back structure show that the reflection coefficient is better than -10 dB from 69 to 86 GHz and the insertion loss for an exclusive transition is 0.65 to 1 dB over the frequency band. Commercial MMIC amplifiers have been integrated with the RGW using the two vertical transitions. The measured results of the integrated MMICs show good performance in terms of small signal gain and bandwidth. The integration of IMGW with MMIC has been realized by utilizing the bond wires and capacitive pads. The measured results show that the amplifier integrated with IMGW has reflection coefficient better than -10 dB and small signal gain larger than 19.5 dB from 73 to 82 GHz.

Author's Contributions: *Proposal of feasible configurations*, *Modelling*, *EM simulation*, *Design optimization*, *Passive measurements*, *Leading role in active measurements*, *Manuscript writing*.

4.2 Paper B

In this chapter, a dual-circularly polarized array antenna based on gap waveguide technology operating at E band has been introduced. The array antenna uses double-grooved circular waveguide polarizer that has two sector grooves placed at 45° and 135° offset from both excitation ports respectively. The operating principles of the polarizer have been presented. Multi-layer design using gap waveguide has been implemented based on the polarizer. A 2×2 unit cell has been presented firstly and optimized for input matching and axial ratios. Then, a 8×8 planar array has been realized. The antenna consists of six layers, including three layers for the feeding networks, one layer for the polarizer, one layer of back cavity and another layer of radiating grid. Corporate feeding networks using folded E-plane T-junctions and H-plane T-

junctions have been presented. The antenna has been fabricated and verified by measurements. The measured results of S-parameters agree well with the simulation and show that reflection coefficients are better than -10 dB for both circular polarizations from 76 to 81 GHz. The measured isolation between the input ports is larger than 25 dB from 76 to 81 GHz. The far-field measurements show that the antenna has realized gain larger than 24 dBi and axial ratios less than 1.5 dB from 76 to 81 GHz.

Author's Contributions: *Proposal of the antenna architecture*, *Modelling*, *EM simulation*, *Design optimization*, *Antenna measurements*, *Manuscript writing*.

4.3 Paper C

Qiannan Ren, Carlo Bencivenni, Giorgio Carluccio, Harshitha Thippur Shivamurthy, Anton de Graauw, Feike Jansen, Jian Yang, Ashraf Uz Zaman
Gapwaveguide Automotive Imaging Radar Antenna With Launcher in Package Technology
IEEE Access, vol. 11, pp. 37483-37493, 2023.
© CCBY-NC-ND DOI: 10.1109/ACCESS.2023.3266958.

An automotive IMR antenna using gapwaveguide technology is presented in this paper. A highly integrated radar transceiver utilizing LiP technology equipped with 4 RXs and 3 TXs is introduced. The transceiver is able to provide RF ports with waveguide interfaces, enabling direct integration with waveguide antennas. Robust interconnects for connecting transceivers to waveguide antennas with non-galvanic contact are proposed using gapwaveguide packaging technology. Compact transitions between RW and RGW are proposed to fan-out the feeding line. Designated antenna elements of the system are realized by slot arrays with center-fed ridge gapwaveguides. Ultimately, the imaging radar antenna has a top radiating slot layer, a middle distribution layer and a bottom interconnect layer capable of accommodating 4 LiP components with considerable assembly tolerance. The interconnects are verified with launchers terminated by short or open loads. Good agreement between the simulation and measurement confirms the expected transmission properties of the interconnects. Input matching and radiation pattern of the

antenna are also verified by measurement. The results indicate that the proposed antenna is able to serve the radar system properly.

Author's Contributions: *Antenna design, Interconnect design, Co-optimization of the interconnect with the LiP transition, Leading role in antenna measurements, Leading role in interconnect measurements, Manuscript writing.*

4.4 Paper D

Qiannan Ren, Olof Eriksson, Carina Marcus, Prateek Thalya, Rustem Elezovic, Carlo Bencivenni, Marcus Hasselblad, Jian Yang, Zhaorui Zang, Ashraf Uz Zaman
An Automotive Polarimetric Radar Sensor with Circular Polarization Based on Gapwaveguide Technology
Submitted to IEEE Transactions on Microwave Theory and Techniques.

This paper presents a novel design of automotive polarimetric radar sensor with circular polarization at 77 GHz band based on gapwaveguide technology. The proposed design employs a MIMO configuration with single-CP TX antennas and dual-CP RX antennas, enabling the acquisition of sufficient polarimetric information while reducing the number of transmitters by half. Gapwaveguide technology is utilized for the implementation of the multi-layer waveguide front-end. Series-fed septum polarizers are employed for the antenna design with low-profile characteristics. Measurement results indicate that the antenna elements enable a high level of cross-polarization across the field of view. Integration of the waveguide front-end with RF boards is achieved using gapwaveguide packaging techniques. Static measurements were conducted on common scattering objects to evaluate the sensor's performance. The results demonstrate that the proposed sensor exhibits superior effectiveness in object identification when compared to conventional radar sensors. Dynamic measurements were performed to evaluate the sensor's Doppler response. The assessments indicate a high level of accuracy, confirming the effectiveness of the proposed sensor in analyzing dynamic movements. Overall, the proposed polarimetric radar sensor provides persuasive evidence that gapwaveguide technology is a highly promising candidate for the realization of advanced automotive radar front-ends.

Author's Contributions: *Proposal of the antenna architecture, Antenna design, Transition design, Antenna measurements, Radar system simulations, Radar measurements in the chamber, Participation of the airfield measurements, Radar measurement data processing, Manuscript writing.*

CHAPTER **5**

Future Works

1. The design of circularly polarized waveguide antennas poses a persistent challenge, particularly when aiming to achieve dual circular polarization. Subsequently, the forthcoming phase of the future work in the context of this thesis research area aims to realize wide-band, low-profile dual circularly polarized waveguide antennas with less number of layers specifically tailored for polarimetric sensing applications. In order to achieve a shared aperture for both the transmitting and receiving antennas, attention must be given to the design of a duplexer that effectively separates the transmitting and receiving signals. This process is essential to minimize the overall form factor of the front-ends.

2. Constrained by the laboratory conditions, the proposed polarimetric radar sensor currently demonstrates poor angular resolution due to the limited availability of transmitters and receivers. Future research in this area aims to explore high-resolution polarimetric sensors that integrate multiple transceivers, enabling the utilization of tens of transmitters and receivers. The incorporation of a large number of transmitters and receivers facilitates the realization of radar sensors with full polarimetric capabilities, thereby enabling the acquisition of comprehensive po-

larimetric information. Nevertheless, it is important to recognize that certain consequential factors, such as increased costs and the need for sophisticated calibration processes, must be carefully addressed throughout the development.

References

[1] SAE International, *Automated driving levels of driving automation are defined in new SAE international standard J3016.* SAE International Warrendale, PA, USA, 2014.

[2] D. J. Yeong, G. Velasco-Hernandez, J. Barry, and J. Walsh, "Sensor and sensor fusion technology in autonomous vehicles: A review," *Sensors*, vol. 21, no. 6, p. 2140, 2021.

[3] J. Steinbaeck, C. Steger, G. Holweg, and N. Druml, "Next generation radar sensors in automotive sensor fusion systems," in *2017 Sensor Data Fusion: Trends, Solutions, Applications (SDF)*, 2017, pp. 1–6.

[4] F. de Ponte Müller, "Survey on ranging sensors and cooperative techniques for relative positioning of vehicles," *Sensors*, vol. 17, no. 2, p. 271, 2017.

[5] Z. Wang, Y. Wu, and Q. Niu, "Multi-sensor fusion in automated driving: A survey," *IEEE Access*, vol. 8, pp. 2847–2868, 2020.

[6] G. Velasco-Hernandez, D. J. Yeong, J. Barry, and J. Walsh, "Autonomous driving architectures, perception and data fusion: A review," in *2020 IEEE 16th International Conference on Intelligent Computer Communication and Processing (ICCP)*, 2020, pp. 315–321.

[7] Continental Automotive, *Short Range Radar – SRR520*, Accessed June 18, 2022.

[8] AutonomouStuff, *Aptiv MRR*, Accessed June 18, 2022.

[9] I. Bilik, S. Villeval, D. Brodeski, *et al.*, "Automotive multi-mode cascaded radar data processing embedded system," in *2018 IEEE Radar Conference (RadarConf18)*, 2018, pp. 0372–0376.

[10] M. Mandlik, V. Brazda, M. Paclik, *et al.*, "Automotive radar – road boundary estimation," in *2021 International Symposium ELMAR*, 2021, pp. 123–126.

[11] G. F. Hamberger, S. Späth, U. Siart, and T. F. Eibert, "A mixed circular/linear dual-polarized phased array concept for automotive radar—planar antenna designs and system evaluation at 78 GHz," *IEEE Transactions on Antennas and Propagation*, vol. 67, no. 3, pp. 1562–1572, 2019.

[12] F. Weishaupt, J. F. Tilly, N. Appenrodt, J. Dickmann, and D. Heberling, "Calibration and signal processing of polarimetric radar data in automotive applications," in *2022 Microwave Mediterranean Symposium (MMS)*, 2022, pp. 1–6.

[13] J. F. Tilly, O. Schumann, F. Weishaupt, J. Dickmann, and G. Wanielik, "Reduction of sidelobe effects in automotive polarimetric radar measurements," in *2021 18th European Radar Conference (EuRAD)*, 2022, pp. 169–172.

[14] J.-S. Lee and E. Pottier, *Polarimetric radar imaging: from basics to applications*. CRC press, 2017.

[15] J. R. Huynen, "Phenomenological theory of radar targets," Ph.D. dissertation, Technische Universiteit Delft, Delft, The Netherlands, 1970.

[16] T. Visentin, "Polarimetric radar for automotive applications," Ph.D. dissertation, Karlsruher Institut für Technologie (KIT), 2019.

[17] O. Auriacombe, V. Vassilev, and N. Pinel, "Dual-polarised radiometer for road surface characterisation," *Journal of Infrared, Millimeter, and Terahertz Waves*, vol. 43, no. 1, pp. 108–124, 2022.

[18] N. Kees and J. Detlefsen, "Road surface classification by using a polarimetric coherent radar module at millimeter waves," in *Proceedings of IEEE National Telesystems Conference - NTC '94*, 1994, pp. 95–98.

[19] V. V. Viikari, T. Varpula, and M. Kantanen, "Road-condition recognition using 24-GHz automotive radar," *IEEE Transactions on Intelligent Transportation Systems*, vol. 10, no. 4, pp. 639–648, 2009.

[20] V. Vassilev, "Road surface recognition at mm-wavelengths using a polarimetric radar," *IEEE Transactions on Intelligent Transportation Systems*, vol. 23, no. 7, pp. 6985–6990, 2022.

[21] S. Trummer, G. F. Hamberger, U. Siart, and T. F. Eibert, "A polarimetric 76–79 GHz radar-frontend for target classification in automotive use," in *2016 European Radar Conference (EuRAD)*, 2016, pp. 346–349.

[22] T. Visentin, J. Hasch, and T. Zwick, "Analysis of multipath and doa detection using a fully polarimetric automotive radar," in *2017 European Radar Conference (EURAD)*, 2017, pp. 45–48.

[23] B. J. Donnet and I. D. Longstaff, "MIMO radar, techniques and opportunities," in *2006 European Radar Conference*, 2006, pp. 112–115.

[24] O. Heaviside, *Electromagnetic theory*. Benn brothers, 1922, vol. 3.

[25] L. Rayleigh, "Xviii. on the passage of electric waves through tubes, or the vibrations of dielectric cylinders," *The London, Edinburgh, and Dublin Philosophical Magazine and Journal of Science*, vol. 43, no. 261, pp. 125–132, 1897.

[26] K. Packard, "The origin of waveguides: A case of multiple rediscovery," *IEEE Transactions on Microwave Theory and Techniques*, vol. 32, no. 9, pp. 961–969, 1984.

[27] C. Bencivenni, A. Haddadi, A. Vosoogh, and M. Hasselblad, "Gapwaveguide technology: A game changer for automotive radars," *MICROWAVE JOURNAL*, vol. 66, no. 1, pp. 22–32, 2023.

[28] M. G. Silveirinha, C. A. Fernandes, and J. R. Costa, "Electromagnetic characterization of textured surfaces formed by metallic pins," *IEEE Transactions on Antennas and Propagation*, vol. 56, no. 2, pp. 405–415, 2008.

[29] D. Sievenpiper, L. Zhang, R. Broas, N. Alexopolous, and E. Yablonovitch, "High-impedance electromagnetic surfaces with a forbidden frequency band," *IEEE Transactions on Microwave Theory and Techniques*, vol. 47, no. 11, pp. 2059–2074, 1999.

[30] A. Vosoogh, A. Haddadi, A. U. Zaman, J. Yang, H. Zirath, and A. A. Kishk, "*W* -band low-profile monopulse slot array antenna based on gap waveguide corporate-feed network," *IEEE Transactions on Antennas and Propagation*, vol. 66, no. 12, pp. 6997–7009, 2018.

[31] J. Liu, A. Vosoogh, A. U. Zaman, and J. Yang, "A slot array antenna with single-layered corporate-feed based on ridge gap waveguide in the 60 GHz band," *IEEE Transactions on Antennas and Propagation*, vol. 67, no. 3, pp. 1650–1658, 2019.

[32] M. Sharifi Sorkherizi, A. Dadgarpour, and A. A. Kishk, "Planar high-efficiency antenna array using new printed ridge gap waveguide technology," *IEEE Transactions on Antennas and Propagation*, vol. 65, no. 7, pp. 3772–3776, 2017.

[33] A. Dadgarpour, N. Bayat-Makou, M. A. Antoniades, A. A. Kishk, and A. Sebak, "A dual-polarized magnetoelectric dipole array based on printed ridge gap waveguide with dual-polarized split-ring resonator lens," *IEEE Transactions on Antennas and Propagation*, vol. 68, no. 5, pp. 3578–3585, 2020.

[34] J. Liu, A. Vosoogh, A. U. Zaman, and J. Yang, "Design and fabrication of a high-gain 60-ghz cavity-backed slot antenna array fed by inverted microstrip gap waveguide," *IEEE Transactions on Antennas and Propagation*, vol. 65, no. 4, pp. 2117–2122, 2017.

[35] A. K. Horestani and M. Shahabadi, "Balanced filter with wideband common-mode suppression in groove gap waveguide technology," *IEEE Microwave and Wireless Components Letters*, vol. 28, no. 2, pp. 132–134, 2018.

[36] A. Vosoogh, M. S. Sorkherizi, A. U. Zaman, J. Yang, and A. A. Kishk, "An integrated ka-band diplexer-antenna array module based on gap waveguide technology with simple mechanical assembly and no electrical contact requirements," *IEEE Transactions on Microwave Theory and Techniques*, vol. 66, no. 2, pp. 962–972, 2018.

[37] A. Vosoogh, M. Sharifi Sorkherizi, V. Vassilev, *et al.*, "Compact integrated full-duplex gap waveguide-based radio front end for Multi-Gbit/s point-to-point backhaul links at E-band," *IEEE Transactions on Microwave Theory and Techniques*, vol. 67, no. 9, pp. 3783–3797, 2019.

[38] E. Rajo-Iglesias, M. Ferrando-Rocher, and A. U. Zaman, "Gap waveguide technology for millimeter-wave antenna systems," *IEEE Communications Magazine*, vol. 56, no. 7, pp. 14–20, 2018.

[39]   A. Vosoogh, P.-S. Kildal, and V. Vassilev, "A multi-layer gap waveguide array antenna suitable for manufactured by die-sink edm," in *2016 10th European Conference on Antennas and Propagation (EuCAP)*, 2016, pp. 1–4.

[40]   Á. Palomares-Caballero, A. Alex-Amor, J. Valenzuela-Valdés, and P. Padilla, "Millimeter-wave 3-D-printed antenna array based on gap-waveguide technology and split E-plane waveguide," *IEEE Transactions on Antennas and Propagation*, vol. 69, no. 1, pp. 164–172, 2021.

[41]   S. Farjana, M. Ghaderi, A. U. Zaman, *et al.*, "Realizing a 140 GHz gap waveguide–based array antenna by low-cost injection molding and micromachining," *Journal of Infrared, Millimeter, and Terahertz Waves*, vol. 42, no. 8, pp. 893–914, 2021, ISSN: 1866-6906.

[42]   S. Farjana, M. Ghaderi, A. U. Zaman, S. Rahiminejad, P. Lundgren, and P. Enoksson, "Low-loss gap waveguide transmission line and transitions at 220–320 GHz using dry film micromachining," *IEEE Transactions on Components, Packaging and Manufacturing Technology*, vol. 11, no. 11, pp. 2012–2021, 2021.

[43]   A. Tamayo-Domínguez, J.-M. Fernández-González, and M. Sierra-Pérez, "Groove gap waveguide in 3-d printed technology for low loss, weight, and cost distribution networks," *IEEE Transactions on Microwave Theory and Techniques*, vol. 65, no. 11, pp. 4138–4147, 2017.

[44]   Texas Instruments, *AWR2243 76-GHz to 81-GHz automotive second-generation high-performance MMIC*, Accessed March 16, 2023.

[45]   Texas Instruments, *AWR1843 Single-chip 76-GHz to 81-GHz automotive radar sensor integrating DSP, MCU and radar accelerator*, Accessed May 12, 2023.

[46]   J. Böck, M. Wojnowski, C. Wagner, *et al.*, "Low-cost eWLB packaging for automotive radar MMICs in the 76–81 GHz range," *International Journal of Microwave and Wireless Technologies*, vol. 5, no. 1, pp. 25–34, 2013.

[47]   Micron Technology, *BGA manufacturer's user guide for Micron BGA parts*, Accessed June 18, 2022.

[48]   Texas Instruments, *AWR1843AOP Single-chip 76-GHz to 81-GHz automotive radar sensor integrating antenna on package, DSP and MCU*, Accessed May 12, 2023.

[49]   Texas Instruments, *AWR6843AOP Single-chip 60-GHz to 64-GHz automotive radar sensor integrating antenna on package, DSP and MCU*, Accessed June 18, 2022.

[50]   S. Dominey, *How AoP technology expands radar sensor placement for automotive applications*, Accessed May 21, 2023.

[51]   H. Winner, S. Hakuli, F. Lotz, and C. Singer, "Handbook of driver assistance systems: Basic information, components and systems for active safety and comfort," *Springer reference*, 2015.

[52]   Texas Instruments, *AWR2243BOOST AWR2243 second-generation 76-GHz to 81-GHz high-performance automotive MMIC evaluation module*, Accessed June 18, 2022.

[53]   F. Jansen, F. Laghezza, S. Alhasson, *et al.*, "Simultaneous multi-mode automotive imaging radar using cascaded transceivers," in *2021 18th European Radar Conference (EuRAD)*, 2022, pp. 441–444.

[54]   Y.-C. Leong and S. Weinreb, "Full band waveguide-to-microstrip probe transitions," in *1999 IEEE MTT-S International Microwave Symposium Digest (Cat. No.99CH36282)*, vol. 4, 1999, 1435–1438 vol.4.

[55]   E. Topak, J. Hasch, and T. Zwick, "Compact topside millimeter-wave waveguide-to-microstrip transitions," *IEEE Microwave and Wireless Components Letters*, vol. 23, no. 12, pp. 641–643, 2013.

[56]   Z. Tong and A. Stelzer, "A vertical transition between rectangular waveguide and coupled microstrip lines," *IEEE Microwave and Wireless Components Letters*, vol. 22, no. 5, pp. 251–253, 2012.

[57]   NXP Semiconductors, *Fully integrated 77 GHz RFCMOS automotive radar transceiver*, Accessed May 12, 2023.

[58]   A. U. Zaman, M. Alexanderson, T. Vukusic, and P.-S. Kildal, "Gap waveguide PMC packaging for improved isolation of circuit components in high-frequency microwave modules," *IEEE Transactions on Components, Packaging and Manufacturing Technology*, vol. 4, no. 1, pp. 16–25, 2014.

[59] A. Bagheri, H. Karlsson, C. Bencivenni, A. Haddadi, T. Emanuelsson, and A. A. Glazunov, "Microstrip to ridge gap waveguide transition for 28 GHz steerable slot array antennas," in *2020 14th European Conference on Antennas and Propagation (EuCAP)*, 2020, pp. 1–4.

[60] A. Bagheri, C. Bencivenni, M. Gustafsson, and A. A. Glazunov, "A 28 GHz 8 × 8 gapwaveguide phased array employing GaN front-end with 60 dBm EIRP," *IEEE Transactions on Antennas and Propagation*, vol. 71, no. 5, pp. 4510–4515, 2023.

[61] A. U. Zaman, P.-S. Kildal, M. Ferndahl, and A. Kishk, "Validation of ridge gap waveguide performance using in-house TRL calibration kit," in *Proceedings of the Fourth European Conference on Antennas and Propagation*, 2010, pp. 1–4.

[62] A. R. Mishra, "Microstrip-to-waveguide transition for 140 GHz using gap waveguide technology," M.S. thesis, Chalmers University of Technology, 2021.

[63] RFbeam Microwave Gmbh, *MR2001_RD Radar Transceiver*, Accessed June 30, 2022.

[64] NXP Semiconductors, *S32R274 End-to-End Reference Design Kit*, Accessed June 18, 2022.

[65] RFbeam Microwave Gmbh, *K-MD2 Engineering Sample*, Accessed June 30, 2022.

[66] Texas Instruments, *MMWCAS-RF-EVM mmWave cascade imaging radar RF evaluation module*, Accessed June 18, 2022.

[67] J. Schoepfel, S. Kueppers, K. Aufinger, and N. Pohl, "A SiGe transceiver chipset for automotive radar applications using wideband modulation sequences," *International Journal of Microwave and Wireless Technologies*, vol. 11, no. 7, pp. 676–685, 2019.

[68] J.-H. Lee, J. M. Lee, K. C. Hwang, D.-W. Seo, D. Shin, and C. Lee, "Capacitively coupled microstrip comb-line array antennas for millimeter-wave applications," *IEEE Antennas and Wireless Propagation Letters*, vol. 19, no. 8, pp. 1336–1339, 2020.

[69] U. Huegel, A. Garcia-Tejero, R. Glogowski, E. Willmann, M. Pieper, and F. Merli, "3D waveguide metallized plastic antennas aim to revolutionize automotive radar," *Microwave Journal*, vol. 65, no. 9, 2022.

[70] G. F. Hamberger, U. Siart, and T. F. Eibert, "A dual-linearly polarized receive antenna array for digital beamforming in automotive use," in *2017 IEEE Asia Pacific Microwave Conference (APMC)*, 2017, pp. 17–20.

[71] S. Trummer, G. F. Hamberger, U. Siart, and T. F. Eibert, "A polarimetrie 76–79 GHz radar-frontend for target classification in automotive use," in *2016 46th European Microwave Conference (EuMC)*, 2016, pp. 1493–1496.

[72] M. Ferrando-Rocher, J. I. Herranz-Herruzo, A. Valero-Nogueira, and B. Bernardo-Clemente, "Dual circularly polarized aperture array antenna in gap waveguide for high-efficiency Ka-band satellite communications," *IEEE Open Journal of Antennas and Propagation*, vol. 1, pp. 283–289, 2020.

[73] I. Nadeem, M. Alibakhshikenari, F. Babaeian, *et al.*, "A comprehensive survey on 'circular polarized antennas' for existing and emerging wireless communication technologies," *Journal of Physics D: Applied Physics*, vol. 55, no. 3, p. 033 002, 2021.

[74] C. Shu, J. Wang, S. Hu, *et al.*, "A wideband dual-circular-polarization horn antenna for mmwave wireless communications," *IEEE Antennas and Wireless Propagation Letters*, vol. 18, no. 9, pp. 1726–1730, 2019.

[75] J. Wu, Y. J. Cheng, H. B. Wang, Y. C. Zhong, D. Ma, and Y. Fan, "A wideband dual circularly polarized full-corporate waveguide array antenna fed by triple-resonant cavities," *IEEE Transactions on Antennas and Propagation*, vol. 65, no. 4, pp. 2135–2139, 2017.

[76] N. Yoneda, R. Miyazaki, I. Matsumura, and M. Yamato, "A design of novel grooved circular waveguide polarizers," *IEEE Transactions on Microwave Theory and Techniques*, vol. 48, no. 12, pp. 2446–2452, 2000.

[77] N. Luo, X. Yu, G. Mishra, and S. K. Sharma, "A millimeter-wave (V-Band) dual-circular-polarized horn antenna based on an inbuilt monogroove polarizer," *IEEE Antennas and Wireless Propagation Letters*, vol. 19, no. 11, pp. 1933–1937, 2020.

[78] I. Agnihotri and S. K. Sharma, "Design of a compact 3-D metal printed Ka-band waveguide polarizer," *IEEE Antennas and Wireless Propagation Letters*, vol. 18, no. 12, pp. 2726–2730, 2019.

[79] C. Shu, S. Hu, X. Cheng, *et al.*, "Wideband dual-circular-polarization antenna with high isolation for millimeter-wave wireless communications," *IEEE Transactions on Antennas and Propagation*, vol. 70, no. 3, pp. 1750–1763, 2022.

[80] U. Balaji and Vahldieck, "Radial mode matching analysis of ridged circular waveguides," *IEEE Transactions on Microwave Theory and Techniques*, vol. 44, no. 7, pp. 1183–1186, 1996.

[81] U. Balaji and R. Vahldieck, "Radial mode matching analysis of ridged circular waveguide," in *Proceedings of 1995 IEEE MTT-S International Microwave Symposium*, 1995, 637–640 vol.2.